Check for updates

AGU ADVANCING EARTH AND SPACE SCIENCES

Water Resources Research

RESEARCH ARTICLE
10.1029/2025WR041324

Field-Scale Soil Moisture Predictions in Real Time Using In Situ Sensor Measurements in an Inverse Modeling Framework: SWIM^2

Marit G. A. Hendrickx[1,2], Jan Vanderborght[1,3], Pieter Janssens[1,4,5], Eric Laloy[6], Sander Bombeke[7], Evi Matthyssen[8], Anne Waverijn[9], and Jan Diels[1,2]

[1]Department of Earth and Environmental Sciences, KU Leuven, Leuven, Belgium, [2]KU Leuven Plant Institute (LPI), KU Leuven, Leuven, Belgium, [3]Agrosphere Institute IBG-3, Forschungszentrum Jülich GmbH, Jülich, Germany, [4]Soil Service of Belgium, Leuven, Belgium, [5]Department of Biosystems, KU Leuven, Leuven, Belgium, [6]Belgian Nuclear Research Center (SCK CEN), Mol, Belgium, [7]Proefstation voor de Groenteteelt, Sint-Katelijne-Waver, Belgium, [8]Praktijkpunt Landbouw Vlaams-Brabant, Herent, Belgium, [9]Viaverda vzw, Kruisem, Belgium

Key Points:

- SWIM^2 predicts soil moisture in agricultural fields using sensor data and unbiased soil sample measurements in Bayesian calibration
- After 20 days of sensor data, SWIM^2 achieves 7-day soil moisture predictions with an accuracy comparable to that of soil moisture sensors
- Unlike classical models, SWIM^2 uses sensor error covariance to provide better uncertainty estimates for decision-making

Supporting Information:

Supporting Information may be found in the online version of this article.

Correspondence to:

M. G. A. Hendrickx,
marit.hendrickx@kuleuven.be

Citation:

Hendrickx, M. G. A., Vanderborght, J., Janssens, P., Laloy, E., Bombeke, S., Matthyssen, E., et al. (2026). Field-scale soil moisture predictions in real time using in situ sensor measurements in an inverse modeling framework: SWIM^2. *Water Resources Research*, *62*, e2025WR041324. https://doi.org/10.1029/2025WR041324

Received 16 JUN 2025
Accepted 15 JAN 2026

Author Contributions:

Conceptualization: Marit G. A. Hendrickx, Jan Vanderborght, Pieter Janssens, Jan Diels
Data curation: Marit G. A. Hendrickx, Pieter Janssens, Sander Bombeke, Evi Matthyssen, Anne Waverijn
Formal analysis: Marit G. A. Hendrickx
Funding acquisition: Marit G. A. Hendrickx, Jan Vanderborght, Pieter Janssens, Jan Diels

© 2026. The Author(s). *Water Resources Research* published by Wiley Periodicals LLC on behalf of American Geophysical Union.
This is an open access article under the terms of the Creative Commons Attribution License, which permits use, distribution and reproduction in any medium, provided the original work is properly cited.

Abstract Affordable autonomous soil sensors and IoT technology enable real-time soil moisture monitoring, which offers opportunities for real-time model calibration and irrigation optimization. We introduce an irrigation decision support system SWIM^2 (Sensor Wielded Inverse Modeling of a Soil Water Irrigation Model), a digital twin that integrates continuous sensor data and unbiased, periodic soil samples with an FAO-based soil water balance model using a Bayesian inverse modeling algorithm, DREAM$_{(ZS)}$ (DiffeRential Evolution Adaptive Metropolis). SWIM^2 estimates 12 soil and crop parameters and their associated probability distributions and correlations, providing soil moisture predictions with uncertainty estimates. The SWIM^2 framework is illustrated and validated in a real-time setup for 18 vegetable cropping cycles on agricultural fields in Flanders, Belgium, with in situ precipitation data. Although using minimal prior knowledge and despite sensor bias, SWIM^2 achieves robust soil moisture predictions for a 7-day horizon, with accuracies comparable to sensor measurements. Predictions improve substantially in precision within the first 20 calibration days and maintain high predictive power throughout the growing season. The impact of in situ measurements and temporal covariance of the observational errors ("error covariance") was assessed, indicating that good knowledge of the error covariance and independent soil moisture samples are essential to correct for sensor bias and ensure accurate model calibration, while continuous sensor data ensure accurate and precise estimates of the dynamics. This study demonstrates the use of soil moisture sensor data in a Bayesian inverse modeling framework, offering practical solutions for real-time soil moisture prediction and irrigation decision-making, enhancing water management across agricultural fields.

Plain Language Summary Advancements in affordable soil sensors and Internet-of-Things (IoT) technology now allow farmers to monitor soil moisture in real time. This opens new possibilities for improving irrigation practices, saving water, and enhancing crop yields. We developed SWIM^2 (Sensor Wielded Inverse Modeling of a Soil Water Irrigation Model), a decision support system that uses real-time soil moisture data from sensors to improve irrigation management. The system combines field measurements with a well-known soil water balance model to estimate 12 key soil and crop parameters. These include factors like how much water the soil can hold and how much water crops use during growth. By using a Bayesian inverse modeling method, SWIM^2 not only predicts soil moisture levels but also provides uncertainty estimates for these predictions, helping farmers make more informed decisions. We tested SWIM^2 in agricultural fields in Flanders, Belgium, and analyzed how accurate and reliable are its predictions at different times during the growth period. Results show high accuracy and precision, and high predictive power after 20 calibration days. This study shows how combining sensor technology with advanced modeling can improve soil moisture predictions and optimize irrigation practices, which in turn could benefit sustainable agriculture and water management.

1. Introduction

1.1. Determining Root Zone (RZ) Soil Moisture for Irrigation Scheduling

The main methods to determine RZ soil moisture are based on soil water balance modeling and in situ soil moisture observations. The latter is generally more accurate and intuitive, while a model can also predict soil

Investigation: Marit G. A. Hendrickx, Jan Vanderborght, Pieter Janssens, Jan Diels
Methodology: Marit G. A. Hendrickx, Jan Vanderborght, Pieter Janssens, Eric Laloy, Sander Bombeke, Evi Matthyssen, Anne Waverijn, Jan Diels
Project administration: Jan Vanderborght, Pieter Janssens, Jan Diels
Resources: Marit G. A. Hendrickx, Jan Vanderborght, Pieter Janssens, Eric Laloy, Sander Bombeke, Evi Matthyssen, Anne Waverijn, Jan Diels
Software: Marit G. A. Hendrickx, Pieter Janssens, Eric Laloy
Supervision: Jan Vanderborght, Pieter Janssens, Jan Diels
Validation: Marit G. A. Hendrickx
Visualization: Marit G. A. Hendrickx
Writing – original draft: Marit G. A. Hendrickx, Jan Vanderborght
Writing – review & editing: Marit G. A. Hendrickx, Jan Vanderborght, Pieter Janssens, Eric Laloy, Evi Matthyssen, Jan Diels

moisture when observations are absent but typically requires knowledge of the crop and soil hydraulic properties. Low resolution soil water balance (SWB) or "bucket" models calculate the amount of water stored in the entire root zone or in limited number of layers that cover the root zone using the law of mass conservation, and assume that water percolates to a deeper layer when field capacity is exceeded (e.g., AquaCrop (Raes et al., 2009; Steduto et al., 2009), BUDGET (Raes, 2002)). In contrast to these simple models, more complex models compute water fluxes based on gradients of water potentials or water contents, for example, by applying Richards' equation (e.g., Hydrus-1D (Simunek et al., 2005), SWAP (Van Dam et al., 1997)), which requires soil water content profiles with high vertical resolution. Distributed models that implement Richards' equation, such as Mike SHE (Butts & Graham, 2005) and MODFLOW 6 (Langevin et al., 2017), further allow for spatially explicit simulations of soil water dynamics at the catchment scale. Simple SWB models have significant potential for irrigation scheduling as they are relatively easy to parameterize and calibrate, and require limited data inputs. These models are also applicable at both small and large scales and integrate well with Internet-of-Things (IoT) technology. In contrast, Richards' equation-based models require extensive input data and computational power as well as more information to calibrate the more complex processes, which limits their applicability in an agricultural context (Pereira et al., 2020).

In recent years, the development of cheap, compact, autonomous soil-based sensors with wireless communication via IoT technology led to real-time access to the soil moisture status of a field (Cahn et al., 2017). Several methods exist to measure soil moisture with soil-based sensors, for example, based on electrical properties of the soil (dielectric permittivity and soil resistivity), soil moisture potential, infrared spectroscopy, and radioactive techniques such as neutron probes. The most commonly used soil moisture sensors measure the dielectric permittivity of a substrate, which is mainly determined by its water content as water has a high relative dielectric permittivity (ε) of around 80, compared to air ($\varepsilon_a = 1$), and soil particles ($\varepsilon_s = 3-6$). Performance and calibration of various dielectric sensors have been studied throughout the past decades (Bircher et al., 2016; Bogena et al., 2017; Dong et al., 2020; George & Soulis, 2012; M. G. A. Hendrickx, Vanderborght, et al., 2025; Kaptein et al., 2019; Nemali et al., 2007; Paige & Keefer, 2008). A sensor is generally provided with a manufacturer's calibration equation, but multiple studies recommend performing a soil-specific or a field-specific sensor calibration to obtain a higher accuracy (Mane et al., 2024; Soulis et al., 2015).

By installing soil moisture sensors, farmers can monitor the soil moisture dynamics and status of their fields in real time, which can help to better understand soil water dynamics and conserve resources (Obaideen et al., 2022). While the agricultural sector is embracing the smart industrial revolution, with farmers gradually adopting innovative technologies to enhance decision-making support (Zambon et al., 2019), they remain hesitant to integrate such sensors in practice (O'Grady & O'Hare, 2017; Thompson et al., 2018). First of all, sensors connected to a datalogger with a communication module can be a costly investment. Additionally, the installation and removal of the sensor modules are labor intensive (Cahn et al., 2017), and the sensor modules are obstacles for management operations in the field. Cahn et al. (2017) also point out that while soil moisture sensors can be valuable for determining the optimal timing to irrigate, they are less effective in estimating the amount of water to apply since this requires additional information on soil water retention properties. Some additional challenges may occur when using soil moisture sensors, such as soil moisture variability across a field, air gaps, representation of a soil layer or RZ, and sensor positioning, specifically in heterogeneously or drip irrigated fields (Soulis et al., 2015).

Several irrigation management decision support systems (DSSs) based on soil water modeling and soil water monitoring exist. In Belgium, Soil Service of Belgium uses a SWB model that is calibrated using soil moisture samples to schedule irrigation in potato, vegetable, and fruit crops (Janssens et al., 2011). El-Naggar et al. (2020) compared a model and sensor-based irrigation DSS in New Zealand and found that the irrigation-water-use efficiency was higher under a sensor-based scheduling regime, which used 27%–45% less water compared to a model-based approach that computed the daily soil-water deficit. Irrigation-Advisor, IRRIX, and Hydro-Tech are other examples of automated water balance-based irrigation scheduling systems relevant in European vegetable production that use in situ soil moisture monitoring or remote sensing (Gallardo et al., 2020), while others predict soil moisture for irrigation decision support tools using machine learning methods (Brinkhoff et al., 2019; W. Wang et al., 2025). Although existing systems often use additional information sources on plant or soil status, they lack robust statistical processing and uncertainty analyses.

19447973, 2026, 2, Downloaded from https://agupubs.onlinelibrary.wiley.com/doi/10.1029/2025WR041324 by Forschungszentrum Jülich GmbH Research Center, Wiley Online Library on [17/05/2026]. See the Terms and Conditions (https://onlinelibrary.wiley.com/terms-and-conditions) on Wiley Online Library for rules of use; OA articles are governed by the applicable Creative Commons License

19447973, 2026, 2, Downloaded from https://agupubs.onlinelibrary.wiley.com/doi/10.1029/2025WR041324 by Forschungszentrum Jülich GmbH Research Center, Wiley Online Library on [17/05/2026]. See the Terms and Conditions (https://onlinelibrary.wiley.com/terms-and-conditions) on Wiley Online Library for rules of use; OA articles are governed by the applicable Creative Commons License

The integration of techniques like Bayesian data assimilation enables automated and improved fusion of soil water modeling, plant sensing, and soil sensing while taking into account measurement uncertainties. Vereecken et al. (2008) highlight the potential of soil moisture measurements for deriving soil hydraulic properties through data assimilation methods, and emphasize that advancements in (soil) hydrology require the integration of improved measurement techniques, (open) data availability, and enhanced modeling methods. These enhanced methods include advanced process models as well as statistical techniques that better account for measurement uncertainty in data assimilation. Such advancements pave the way for autonomous irrigation scheduling systems driven by enhanced soil moisture simulations and predictions.

1.2. Bayesian Inference for Inverse Problems in Hydrology and Agriculture

An inverse problem can be defined as a framework where observations are translated into information about the process or system that produced these observations, for example, soil moisture observations are translated into information on soil properties or evapotranspiration. In Bayesian inference, an inverse problem is solved by updating a prior distribution of a model state or parameter, based on observations. The prior distribution can either be non-informative, such as a uniform distribution where only the lower and upper boundary are known, or informative, such as a normal distribution, if there is already a reasonable understanding of the state's or parameter's likely distribution before applying Bayesian inference. The posterior distribution can be derived by adopting Bayes' theorem (Equation 1):

$$p(\mathbf{A}|\mathbf{B}) = \frac{p(\mathbf{A})\, p(\mathbf{B}|\mathbf{A})}{p(\mathbf{B})}, \tag{1}$$

where $\mathbf{A}$ signifies a vector of model states or parameters, with $p(\mathbf{A})$ being the prior probability distribution, while $\mathbf{B}$ signifies a vector of observations, with $p(\mathbf{A}|\mathbf{B})$ being the posterior or conditional probability distribution, $p(\mathbf{B}|\mathbf{A}) \equiv L(\mathbf{A}|\mathbf{B})$ being the likelihood of $\mathbf{A}$ given $\mathbf{B}$, and $p(\mathbf{B})$ the marginal probability distribution, which acts as a normalizing constant.

Solving inverse problems with Bayesian inference requires an efficient sampling method to explore high-dimensional posterior distributions. Markov Chain Monte Carlo (MCMC) is widely used for this purpose, generating correlated sequences of samples (Markov chains) based on previous values, in contrast to classical Monte Carlo methods that draw independent samples. After a burn-in period, the chains converge to the target distribution. Among adaptive MCMC algorithms, DREAM$_{(ZS)}$ stands out for its use of multiple chains, subspace sampling, and an archive of past states, which significantly improve convergence and sampling efficiency (Laloy & Vrugt, 2012; Vrugt, 2016). Recent studies show that DREAM$_{(ZS)}$ consistently outperforms alternatives like Metropolis-Hastings and adaptive Metropolis, especially in high-dimensional and complex settings (Kavianihamedani et al., 2024).

DREAM has already been applied repeatedly to inverse problems in the context of hydrology and earth sciences. Laloy et al. (2010) assessed parameter uncertainty and its effects on model predictions for a continuous, plot-scale, rainfall–runoff model with DREAM. Dumont et al. (2014) used DREAM$_{(ZS)}$ for parameter estimation of the STICS crop model using biomass measurements. Furthermore, DREAM$_{(ZS)}$ was recently used to calibrate radiative transfer model parameters related to vegetation and surface soil moisture based on Sentinel-1 satellite backscatter observations (De Lannoy et al., 2024; de Roos et al., 2023). In addition to model parameters, also forcing data errors can be assessed by DREAM as was demonstrated by Vrugt et al. (2008) for a watershed model calibration. The posterior distribution of watershed model parameters was significantly modified by addressing these forcing errors during the calibration process.

Several studies in soil hydrology (Jacques et al., 2002; Ritter et al., 2003; X. Wang et al., 2021; Wöhling & Vrugt, 2011; Wöhling et al., 2008) suggest that in situ observations often contain insufficient information to accurately estimate soil hydraulic properties in Richards' equation-based models. In contrast, simple SWB models typically require fewer parameters and input data than transient models for their parameters to be well resolved during calibration. It is therefore particularly relevant to assess whether these simple SWB models can reliably predict the temporal evolution of RZ soil moisture after parameter estimation.

An additional difficulty in the application of Bayesian inverse modeling in an agricultural context is the restricted availability of observational data. In farmers' fields, only a very limited number of sensors can be installed due to

19447973, 2026, 2, Downloaded from https://agupubs.onlinelibrary.wiley.com/doi/10.1029/2025WR041324 by Forschungszentrum Jülich GmbH Research Center, Wiley Online Library on [17/05/2026]. See the Terms and Conditions (https://onlinelibrary.wiley.com/terms-and-conditions) on Wiley Online Library for rules of use; OA articles are governed by the applicable Creative Commons License

costs and operational limitations, typically much less than in experimental fields or studies. Such a setup may result in significant observational errors, that is, deviations from the true soil water content (SWC), which can be systematic and random errors resulting from instrumental and representational errors. When spatial coverage of sensor measurements is limited, the average SWC measurement may be biased compared to the true average SWC in the measurement zone (MZ). Such a bias, or systematic error, is a consistent error over time, and can thus be described as errors that are temporally correlated. It is important to assess and quantify these errors when the observations are used in a Bayesian inverse modeling framework. While model error covariance has been well studied (Bannister, 2008; Goux et al., 2025), observational error covariance has received less attention. Although hydrological inverse modeling, data assimilation, and validation often neglect observational error autocorrelation, ignoring or underestimating this autocorrelation can lead to bias and an underestimation of the uncertainty in model predictions when calibrating to a time series of soil moisture measurements. Some approaches explicitly account for autocorrelated observational errors using autoregressive models (Engeland & Gottschalk, 2002; Evin et al., 2013; Scharnagl et al., 2015), or correct bias via CDF matching (Reichle & Koster, 2004). Estimating observation and model biases simultaneously with the state variables can improve accuracy, whereas neglecting correlations can propagate errors in both state and bias estimates (Crow & Van Loon, 2006; Pauwels & De Lannoy, 2015; Pauwels et al., 2013). A common workaround is inflating error variances to compensate for neglected correlations, but this compromises accuracy (Hu & Dance, 2024; Stewart et al., 2008). Previous studies propose mechanistic error modeling based on the spatial variability of soil properties (M. G. A. Hendrickx et al., 2023), and statistically pooled error modeling based on measurements and their observational errors in multiple fields (M. G. A. Hendrickx et al., 2025). A challenge related to this is how sensor measurement uncertainty can be mitigated by incorporating additional soil moisture sampling campaigns, which occur at much lower frequencies but provide unbiased measurements with a low uncertainty.

1.3. Objectives

This study presents the development and evaluation of SWIM^2 (Sensor Wielded Inverse Modeling of a Soil Water Irrigation Model), a real-time irrigation decision support system (DSS). The SWIM^2 framework uses in situ soil moisture measurements to calibrate 12 parameters of a SWB model with DREAM$_{(ZS)}$, to predict SWC and its uncertainty over a 7-day horizon. In operational mode, SWIM^2 is to be applied once or twice per week for each individual field.

The specific objectives of this study are

1. To calibrate a low-dimensional SWB model that integrates in situ samples and sensor data, after applying a generalized sensor calibration, while incorporating measurement error covariance, in order to accurately describe and predict soil moisture dynamics and their uncertainty.
2. To evaluate the influence of measurement error covariance on model calibration and uncertainty estimates within a Bayesian inverse modeling framework.
3. To assess the impact of periodic, unbiased soil moisture samples versus continuous sensor data on the accuracy and predictive power of the model within a Bayesian inverse modeling framework, and to establish the optimal sample quantity or frequency required for effective model calibration.

In line with these objectives, our main goal is thus to propose a low-cost, user-friendly soil moisture prediction and irrigation management DSS tailored for farmers. When time and money are not limited, a dense sensor network can be deployed, high measurement accuracy can be ensured, and observational error assessment becomes trivial. In contrast, we investigate the potential and challenges of using a measurement setup with only three low-cost soil moisture sensors, providing limited spatial coverage within a MZ, to support accurate soil moisture modeling and irrigation decision-making.

2. Study Sites and Data

2.1. Study Sites

A total of 18 cropping cycles during the growing seasons of 2021–2023 were used in this study for the illustration and validation of the SWIM^2 framework. The study sites (Figure 1) were located at Kinrooi and three research centers in Flanders, Belgium (*Viaverda* in Kruisem, *Proefstation voor de Groenteteelt* in Sint-Katelijne-Waver, and *Praktijkpunt Landbouw Vlaams-Brabant* in Herent), where various types of vegetable crops were grown,

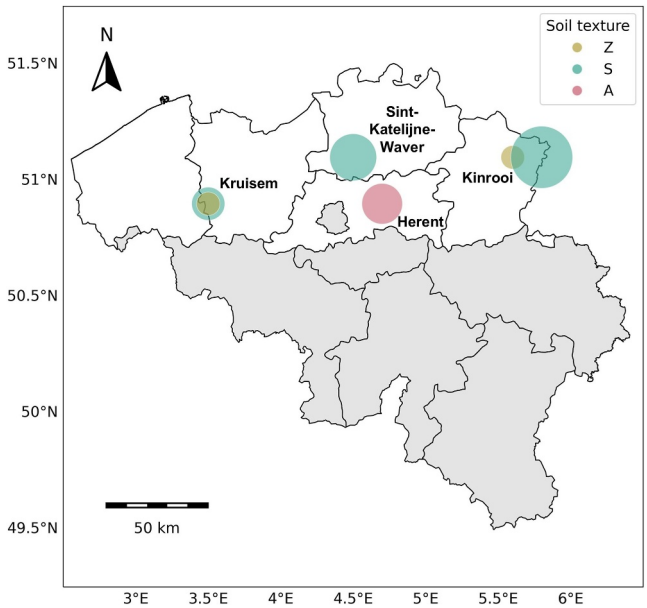

Figure 1. Map of the study sites in Flanders, the northern part of Belgium, indicated by their soil type (Belgian soil classification: Z: sand, S: loamy sand, A: silt loam), and number of cropping cycles (size). A total of 18 cropping cycles during the growing seasons of 2021–2023 were used in this study, including 8 cropping cycles in Kinrooi, 4 cropping cycles in Sint-Katelijne-Waver, 3 cropping cycles in Herent, and 3 cropping cycles in Kruisem. Of these cropping cycles, 2 were on a sand soil (Z) and 3 on a silt loam soil (A), while the majority of 13 cropping cycles were on loamy sand soils (S).

including onions, celery, leek and Belgian endive, and irrigation was applied based on irrigation advice from Soil Service of Belgium.

2.2. Weather Data

Weather data for the study sites were obtained from two main sources. Precipitation was measured in situ at each site using a tipping-bucket rain gauge. To complement these measurements, precipitation radar data were retrieved and used to correct for false zeros and to fill occasional gaps. For the remaining weather variables (temperature, wind speed, relative humidity, air pressure, sunshine duration, solar radiation, and cloudiness), data were collected from the nearest Royal Meteorological Institute (RMI) synoptic weather station via the OpenKMI python package. The 22 synoptic weather stations are on average 20 km apart. With these weather parameters, daily reference potential evapotranspiration, ETo, was calculated based on the FAO-56 Penman-Monteith method (Allen et al., 1998), using the PyETo python package (Richards, 2015).

The precipitation data from the site-specific rain gauges were highly reliable, except for occasional missing values, which were effectively corrected using radar products. The other meteorological variables obtained from the nearest synoptic stations are also considered reliable, though spatial representativeness may decrease with increasing distance from the experimental fields. In contrast to precipitation, ETo varies smoothly across Flanders due to its flat topography and relatively homogeneous climate, and differences between synoptic stations are generally small compared to the variability in precipitation, irrigation, soil and crop management.

2.3. Soil Analysis

To determine soil characteristics, three undisturbed Kopecky ring samples (V: 100 cm^3, h: 51 mm) were collected within the MZ of each study site at the start of the growing period. Soil water retention was measured at various matric potentials using the pressure plate method, which provided the saturation point at pF 0 (pF $= \log_{10}(|h|)$ where h is the soil water pressure head expressed in cm), theoretical field capacity at pF 2, critical threshold at pF 2.7, and permanent wilting point at pF 4.2. Finally, the ring samples were dried to determine dry bulk density (BD). Occasionally, granulometry was performed, obtaining a more accurate soil texture classification.

2.4. In Situ Soil Moisture Samples

A composite soil moisture sample, consisting of nine individual gouge auger soil samples (0–30 cm depth and 2 cm diameter) spatially distributed over an 80 m^2 MZ, was collected periodically at all sites during the growing period. The standard deviation of 0.0114 m^3 m^{-3} reflects the spatial variability among the individual samples within the measurement zone, and was calculated as a pooled standard deviation across multiple study sites (M. G. A. Hendrickx et al., 2025). The sampling errors of the subsequent sampling campaigns are uncorrelated, since the individual samples were spatially randomized during each campaign. The soil moisture content of the composite samples was determined using the gravimetric method, with drying to constant weight ensuring unbiased readings. Subsequently, the volumetric water content (θ_{vol}) was calculated from the gravimetric water content (θ_{grav}) and BD:

$$\theta_{vol} = \theta_{grav} \times \mathrm{BD}. \quad (2)$$

Any systematic error associated with the sampling and gravimetric measurement technique itself was assumed to be negligible.

19447973, 2026, 2, Downloaded from https://agupubs.onlinelibrary.wiley.com/doi/10.1029/2025WR041324 by Forschungszentrum Jülich GmbH Research Center, Wiley Online Library on [17/05/2026]. See the Terms and Conditions (https://onlinelibrary.wiley.com/terms-and-conditions) on Wiley Online Library for rules of use; OA articles are governed by the applicable Creative Commons License

19447973, 2026, 2, Downloaded from https://agupubs.onlinelibrary.wiley.com/doi/10.1029/2025WR041324 by Forschungszentrum Jülich GmbH Research Center, Wiley Online Library on [17/05/2026]. See the Terms and Conditions (https://onlinelibrary.wiley.com/terms-and-conditions) on Wiley Online Library for rules of use; OA articles are governed by the applicable Creative Commons License

2.5. In Situ Soil Moisture Sensors

Dielectric capacitance soil moisture sensors (TEROS 10, Meter Group, Inc., USA) were used to measure volumetric SWC in the fields. The sensors use an electromagnetic field to measure the dielectric permittivity of the surrounding medium within a measurement volume of 430 mL, approximately corresponding to a cylinder with a diameter of 7.1 cm and a height of 10.9 cm. A 70 MHz oscillating wave is supplied to the two sensor needles, which charge according to the dielectric permittivity of the material. The charge time is proportional to the dielectric permittivity, and hence water content, of the soil. Raw sensor output [mV] was converted to SWC $\left[\mathrm{m}^3\ \mathrm{m}^{-3}\right]$ using the manufacturer's calibration equation, with a stated accuracy of 0.03 $\mathrm{m}^3\ \mathrm{m}^{-3}$ (METER Group, 2018):

$$\theta_{\mathrm{sensor}} = -2.154 + 3.898 \times 10^{-3} \times S_{\mathrm{mV}} - 2.278 \times 10^{-6} \times {S_{\mathrm{mV}}}^2 + 4.824 \times 10^{-10} \times {S_{\mathrm{mV}}}^3, \quad (3)$$

where S_{mV} is the raw sensor output [mV], and θ_{sensor} is the volumetric water content $\left[\mathrm{m}^3\ \mathrm{m}^{-3}\right]$. Decagon 10HS and 5TE sensors, the predecessors of the TEROS high-frequency capacitance soil moisture sensors, have been evaluated in previous studies (Varble & Chávez, 2011; Vaz et al., 2013). More recently, Nasta et al. (2024) investigated temperature effects on the calibration of comparable sensors (GS3 and TEROS 12, METER Group) and found that applying a temperature correction improved accuracy, especially in clay-rich soils.

A sensor module that was installed in a field (AgriSense Pro, Io-Things, Belgium) comprises three TEROS 10 sensors connected via cable to a datalogger with a Sigfox communication module. The communication module transmits sensor data to an online server for real-time online data access. The temporal resolution of the sensor measurements was reduced to daily observations by selecting the last measurement of each day, which typically occurred between 22:00 and 00:00, as the soil water balance model computes a daily water balance at the end of the day. Finally, the daily measurements of the three sensors were averaged.

The general sensor calibration of M. G. A. Hendrickx et al. (2025) was applied to eliminate the discrepancy between a point measurement of a sensor with the pins installed horizontally at 15 cm depth and a soil sample measuring the whole upper 30 cm layer, obtaining sensor measurement data that are representative for the 0–30 cm soil layer. This calibration curve (Equation 4) was previously established based on an orthogonal fit of soil moisture sample measurements of the 0–30 cm layer to their corresponding sensor measurements at 15 cm depth at multiple study sites in 2021, 2022 and 2023.

$$\theta_{0-30\ \mathrm{cm}} = -0.006 + \overline{\theta}_{\mathrm{sensor}} \times 1.26, \quad (4)$$

where $\theta_{0-30\ \mathrm{cm}}$ $\left[\mathrm{m}^3\mathrm{m}^{-3}\right]$ is the volumetric SWC in the 0–30 cm soil layer, and $\overline{\theta}_{\mathrm{sensor}}$ $\left[\mathrm{m}^3\mathrm{m}^{-3}\right]$ is the average volumetric SWC, that is, measured by the three sensors at 15 cm depth. The calibration curve had an R^2 of 0.67 and an RMSE of 0.043 $\mathrm{m}^3\ \mathrm{m}^{-3}$ (M. G. A. Hendrickx et al., 2025).

In contrast to composite soil samples, the averaged sensor measurements may be biased relative to the true average soil moisture content of the 80 m^2 MZ since three point measurements may not adequately represent the entire MZ. As a result, deviations of the averaged sensor measurements from the true soil moisture are persistent in time. Such persistence can either be addressed by explicitly considering the autocorrelated errors, or by introducing a bias term as an additional unknown parameter. In a real-time context, however, unbiased measurements are sparse and become available only during the growing season, preventing accurate quantification of this bias, which is why we chose to adopt the full error covariance structure.

3. Methods

3.1. Soil Water Balance Model

A single-layered soil water balance "bucket" model, based on FAO-56 approaches (Allen et al., 1998), computes a daily soil water balance for the growing RZ using weather data, soil and crop parameters as input. The model assumes a uniform SWC throughout the RZ and does not account for lateral flow. The soil water balance model applies a dual crop coefficient, as is recommended for real-time irrigation scheduling with high frequency water

19447973, 2026, 2, Downloaded from https://agupubs.onlinelibrary.wiley.com/doi/10.1029/2025WR041324 by Forschungszentrum Jülich GmbH Research Center, Wiley Online Library on [17/05/2026]. See the Terms and Conditions (https://onlinelibrary.wiley.com/terms-and-conditions) on Wiley Online Library for rules of use; OA articles are governed by the applicable Creative Commons License

applications. The complete description of the model can be found in Text S1 of Supporting Information S1: Soil water balance model.

While a single-layered soil water model approach offers conceptual simplicity and requires calibration of only a few parameters, challenges may arise when comparing the water content in the single-layered soil water model, which is derived from the soil water storage and from the thickness of the single soil layer assuming a vertically uniform water content distribution, with in situ measurements when the actual water content distribution is not uniform with depth. A first situation that poses such a challenge is when the RZ extends and grows into soil layers below the upper 30 cm thick soil layer, which is monitored by the soil sensors. Since no water was extracted from the deeper soil layer before roots grew into it, the water content in the deeper soil layer is initially higher than in the upper soil layer in which the water content is monitored. A second situation posing a challenge is when precipitation or irrigation water is added to the upper soil layer but does not distribute immediately into the deeper soil layer and deeper part of the RZ where water contents are not monitored. To allow comparison of model simulations and measurements in the top 30 cm layer, the single-layered soil water model was modified implementing a virtual RZ, that is, linked to a dual-layer conceptual framework (layer 1: 0–30 cm; layer 2: 30 cm —maximum root depth) (Text S.1.6 in Supporting Information S1). When the actual RZ grows into deeper and wetter soil layers, the available water in the RZ soil layer will increase but this increase will not change the top 30 cm SWC. Therefore, the virtual RZ layer with uniform water content that corresponds with the water content in the upper 0–30 cm layer will be expanded more than the actual RZ in order to account for the stronger increase in soil water in the root zone due to root growth in the wetter subsoil. Vice versa, when the water content in the monitored topsoil layer increases after a rainfall or irrigation event but when the water is not immediately distributed over the whole RZ, the virtual RZ layer of the single layer model is compressed to maintain the measured SWC in layer 1 and a correct water storage in the virtual RZ. The dual-layer conceptual model links the virtual RZ depth, the actual RZ depth, and the water contents in the upper and deeper soil layer with each other.

Initial estimates for the basal crop coefficient, K_{cb}, of non-stressed, well-managed crops in sub-humid climates ($RH_{min} \approx 45\%$, $u_2 \approx 2$ m s^{-1}), such as Flanders, as well as the maximum effective rooting depth, $Z_{r,max}$, and the lengths of crop development stages, L, were derived from the tables in the FAO-56 Irrigation and Drainage Paper (Allen et al., 1998) and adjusted based on local expert knowledge of Soil Service of Belgium. The crop-specific soil water depletion fractions, p, for no stress and for $ET_m \approx 5$ mm day^{-1} were extracted from the FAO-56 Irrigation and Drainage Paper (Allen et al., 1998). For each field, one or two cultivations per year were included, of which the crop and the planting or sowing date were marked up.

3.2. Bayesian Approach for Inverse Modeling

3.2.1. DREAM$_{(ZS)}$

In this study, the soil water balance model described in Section 3.1 was coupled with the DREAM$_{(ZS)}$ algorithm (Laloy & Vrugt, 2012; Ter Braak & Vrugt, 2008; Vrugt et al., 2009). A Python 3 implementation was used, based on the 2013 DREAMzs Matlab code (version 1.5, licensed under GPL3). Vrugt (2016) provides an overview of hyperparameters and possible configurations of the various DREAM variants. Twelve uncertain parameters of the soil water balance model were estimated using DREAM$_{(ZS)}$ and nine parameters were obtained from measurements or literature. The choice of six independent chains (N) was determined based on the dimensionality (d), ensuring $N \geq 0.5d$. Although sequential data assimilation approaches (e.g., filters) are commonly used in real-time contexts, we adopted DREAM$_{(ZS)}$ to exploit the full observation time series for Bayesian parameter inference and uncertainty quantification, which is expected to provide more robust parameter estimates and predictions. The configuration of the DREAM$_{(ZS)}$ is elaborated on in Appendix B.

3.2.2. Likelihood Function

The loglikelihood (LL) is a key objective function in Bayesian inverse modeling, summarizing the deviations between model simulations and corresponding observations. For uncorrelated heteroscedastic error residuals $\mathbf{E}(\mathbf{x}) = \mathbf{Y}(\mathbf{x}) - \tilde{\mathbf{Y}}$, the LL can be defined by Equation 5 (Vrugt, 2016).

$$\mathcal{L}\left(\mathbf{x}; \tilde{\mathbf{Y}}, \boldsymbol{\sigma}^2\right) = -\frac{n}{2}\ln(2\pi) - \frac{1}{2}\sum_{t=1}^{n}\left\{\ln\left(\hat{\sigma}_t^2\right)\right\} - \frac{1}{2}\sum_{t=1}^{n}\left(\frac{y_t(\mathbf{x}) - \tilde{y}_t}{\hat{\sigma}_t}\right)^2, \quad (5)$$

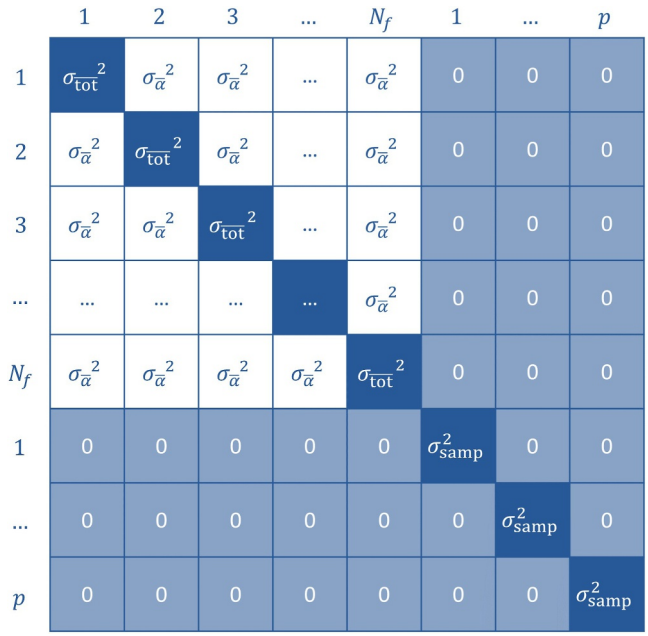

Figure 2. Pooled measurement error covariance matrix for N_f daily sensor measurements and p samples (M. G. A. Hendrickx et al., 2025).

where n is the number of simulation-observation pairs, $\mathbf{x}$ is the parameter set with d parameters resulting in a vector $\mathbf{Y}(\mathbf{x})$ of model simulations $(y_1, y_2, \ldots, y_n)$, $\widetilde{\mathbf{Y}}$ is a vector of the corresponding observations $(\tilde{y}_1, \tilde{y}_2, \ldots, \tilde{y}_n)$ and $\boldsymbol{\sigma}$ is a vector of their standard deviation $(\hat{\sigma}_1, \hat{\sigma}_2, \ldots, \hat{\sigma}_n)$ arising from observational errors. When the error residuals $\mathbf{E}(\mathbf{x})$ exhibit correlation, the LL function can be expanded to Equation 6.

$$\mathcal{L}\left(\mathbf{x}; \widetilde{\mathbf{Y}}, \boldsymbol{\Sigma}\right) = -\frac{n}{2}\ln(2\pi) - \frac{1}{2}\ln(|\boldsymbol{\Sigma}|) - \frac{1}{2}\left(\mathbf{Y}(\mathbf{x}) - \widetilde{\mathbf{Y}}\right)^{\mathrm{T}} \boldsymbol{\Sigma}^{-1} \left(\mathbf{Y}(\mathbf{x}) - \widetilde{\mathbf{Y}}\right), \quad (6)$$

where $\boldsymbol{\Sigma}$ is the measurement error covariance matrix.

Our approach assumes that deviations between model simulations and corresponding observations arise solely from observational errors. Equations 5 and 6 therefore evaluate how plausible it is to observe such deviations under the (naive) assumption that the model perfectly describes reality for a given parameter set $\mathbf{x}$, while accounting for the known characteristics of the observational errors, that is, their variance and autocorrelation.

3.2.3. Measurement Error Covariance Matrix

Accurate (inverse) modeling of soil moisture requires a good understanding of errors in observational data. These errors can be categorized into random errors and systematic errors. Random errors, which arise due to unpredictable variations during measurements, are uncorrelated across observations over time. Systematic errors, in contrast, are consistent deviations affecting all subsequent measurements in a similar way. Such systematic errors can include both additive (intercept) errors, which shift all measurements by a constant amount, and multiplicative (slope) errors, which scale measurements proportionally. In this study, only additive systematic errors are considered. The temporal correlation of the systematic errors is captured in the error covariance matrix, while the sum of the random and systematic errors forms the total observational error variance.

However, accurately quantifying measurement error variance and covariance is particularly challenging in practical field setups where typically only three sensors per field are available. To estimate the measurement error covariance matrix ($\boldsymbol{\Sigma}$), we employed a pooled error modeling framework that integrates sparse measurements across multiple fields, leveraging their shared statistical properties to separate random and systematic error components (M. G. A. Hendrickx et al., 2025). In this approach, we assume that the measurement error covariance matrix is applicable across fields and soil types, for a specific measurement setup.

The measurement error covariance matrix ($\boldsymbol{\Sigma}$),was quantified for our specific measurement setup based on averaged sensor measurements as described by (M. G. A. Hendrickx et al., 2025; Figure 2). The variance of the systematic error, or error covariance, $(\sigma_{\overline{\alpha}}{}^2)$ was assumed to be the same for all sensor measurement pairs and was 0.00107 $\left(\sigma_{\overline{\alpha}} = 0.033\ \mathrm{m^3\ m^{-3}}\right)$. This assumption implies the presence of a constant bias $\overline{\alpha}$ in averaged sensor measurements within a certain field that does not vary over time, and implies that the biases across different fields originate from the same population $\mathcal{N}\left(0, \sigma_{\overline{\alpha}}{}^2\right)$. The random error variance $(\sigma_{\overline{\epsilon}}{}^2)$ was $0.00100\left(\sigma_{\overline{\epsilon}} = 0.032\ \mathrm{m^3\ m^{-3}}\right)$, implying that all random errors $\overline{\epsilon}$ originate from the population $\mathcal{N}\left(0, \sigma_{\overline{\epsilon}}{}^2\right)$ The total error variance $\left(\sigma_{\overline{tot}}{}^2\right)$, that is, the sum of the systematic and random error variance:

$$\sigma_{\overline{tot}}{}^2 = \sigma_{\overline{\alpha}}{}^2 + \sigma_{\overline{\epsilon}}{}^2, \quad (7)$$

was 0.00207 $\left(\sigma_{\overline{tot}} = 0.045\ \mathrm{m^3\ m^{-3}}\right)$. These error variances correspond to a substantial error correlation of 0.52, indicating that approximately half of the sensor observational error variance is attributed to systematic deviations (M. G. A. Hendrickx et al., 2025). In this context, measurement accuracy refers to how close the average of sensor measurements is to the true soil moisture value. It is influenced by both systematic and random errors that affect the average measurement. Measurement precision, on the other hand, refers to how consistent and repeatable the

19447973, 2026, 2, Downloaded from https://agupubs.onlinelibrary.wiley.com/doi/10.1029/2025WR041324 by Forschungszentrum Jülich GmbH Research Center, Wiley Online Library on [17/05/2026]. See the Terms and Conditions (https://onlinelibrary.wiley.com/terms-and-conditions) on Wiley Online Library for rules of use; OA articles are governed by the applicable Creative Commons License

19447973, 2026, 2, Downloaded from https://agupubs.onlinelibrary.wiley.com/doi/10.1029/2025WR041324 by Forschungszentrum Jülich GmbH Research Center, Wiley Online Library on [17/05/2026]. See the Terms and Conditions (https://onlinelibrary.wiley.com/terms-and-conditions) on Wiley Online Library for rules of use; OA articles are governed by the applicable Creative Commons License

Table 1
Model Parameters and Their Ranges, Where i Is the Prior Estimate of the Respective Parameter

Parameter	Definition	Lower boundary	Upper boundary
$K_{cb,ini}$	K_{cb} during initial stage [−]	0.05	0.4
$K_{cb,mid}$	K_{cb} during mid-season stage [−]	0.85	1.15
$K_{cb,end}$	K_{cb} at the end [−]	0.65	1.15
L_{ini}	Length of initial stage [days]	$\max(i - 10, 0)$[a]	$i + 10$
L_{dev}	Length of development stage [days]	$\max(i - 7, 0)$	$i + 7$
L_{mid}	Length of mid-season stage [days]	$\max(i - 7, 0)$	$i + 7$
θ_{FC}	Field capacity (FC) [$m^3 m^{-3}$]	$\min(i, 0.15)$	$\min(0.4, i + 0.25)$[b]
$\ln(K_{sat})$	Natural logarithm of K_{sat} [mm day^{-1}]	$\ln(K_{sat,min})$	$\ln(K_{sat,max})$
CN	Curve number [−]	58	91
$z_{GWT,max}$	Maximum groundwater table depth [cm]	100	200
$z_{r,max}$	Maximum root depth [m]	0.3	0.9
θ_{ini}	Initial SWC [$m^3 m^{-3}$]	0.1	$\min(0.4, i + 0.25)$

[a]For Belgian endive, the lower boundary of $L_{ini} = \max(i - 21, 0)$ as the complete initial stage may be long, but the emergence stage of the seed is not included in the measurement data. [b]Field capacity was not expected to exceed 0.4 m^3 m^{-3} since clayey soils were not included in this study.

individual sensor readings are, and is mainly affected by the random and systematic errors of each individual measurement.

Because of the way soil moisture samples were taken at different sampling times (Section 2.4), their errors are uncorrelated over time as well as uncorrelated to the sensor measurement errors. The standard deviation of an individual soil moisture sample was 0.0114 m^3 m^{-3}. For a composite soil moisture sample comprising n individual soil samples, the standard deviation reduces to $0.0114\, n^{-1/2}$. For $n = 9$, this results in a standard deviation of 0.0038 m^3 m^{-3}, which corresponds to a variance of $\sigma^2_{samp} = 0.0000144$.

The final error covariance matrix for a given field f has $(N_f + p)$ rows and columns with N_f being the number of averaged sensor measurements and p being the number of uncorrelated composite soil moisture samples (Figure 2).

3.2.4. Prior Parameter Information

In this study, prior parameter distributions were specified as bounded non-informative priors, that is, uniform with strict lower and upper bounds, chosen to reflect the feasible physical range of each parameter. While such priors can become informative if the posterior accumulates near a boundary, they were intended here as weakly informative constraints in the absence of detailed a priori knowledge. The initial states of the chains were randomly sampled from these prior distributions with Latin Hypercube Sampling (LHS).

All 12 uncertain model parameters that are estimated in $DREAM_{(ZS)}$ are shown in Table 1, along with the lower and upper boundary of their uniform prior distribution. The lower and upper boundary of K_{sat} ($K_{sat,min}$ and $K_{sat,max}$, respectively) are defined per soil textural class (Text S1: Table S1 in Supporting Information S1). The boundaries of CN (curve number) are based on values proposed by the Soil Conservation Service (SCS) (1964), assuming row crops and legumes, and including all hydrological soil groups. The lower and upper boundary of the maximum groundwater table depth are assumed to be location-independent, and the groundwater is expected to be above 200 cm depth for the agricultural fields in this study.

The boundaries of the basal crop coefficients (K_{cb}) and the maximum rooting depth are based on FAO-56 (Allen et al., 1998). These crop parameter boundaries are defined independently from the crop type since vegetable crops generally have similar characteristics, and differences between vegetable crops are expected to be smaller compared to differences in growth and canopy cover due to environmental factors. The boundaries of the growth stage lengths are defined as crop-dependent since these differ more substantially between different vegetable

crops. The prior estimates of the growth stage lengths can be found in Text S1: Table S1 of Supporting Information S1. The prior estimate of FC was based on the measured soil moisture content at pF 2. The prior estimate of θ_{ini} was set to the prior estimate of FC.

3.2.5. Posterior Parameter Distribution

The posterior distribution of the parameters is derived by adopting the Bayesian approach:

$$p\left(\mathbf{x}|\widetilde{\mathbf{Y}}\right) = \frac{p(\mathbf{x})\, p\left(\widetilde{\mathbf{Y}}|\mathbf{x}\right)}{p\left(\widetilde{\mathbf{Y}}\right)}, \tag{8}$$

where $\mathbf{x}$ signifies a vector of parameters $(x_1, x_2, \ldots, x_d)$, with $p(\mathbf{x})$ being the prior parameter distribution, while $\widetilde{\mathbf{Y}}$ signifies a vector of soil moisture measurements, with $p\left(\mathbf{x}|\widetilde{\mathbf{Y}}\right)$ being the posterior parameter distribution, $p\left(\widetilde{\mathbf{Y}}|\mathbf{x}\right) \equiv L\left(\mathbf{x}|\widetilde{\mathbf{Y}}\right)$ being the likelihood function and $p\left(\widetilde{\mathbf{Y}}\right)$ the marginal likelihood, which is a normalizing constant. As a uniform prior is used, this is reduced to:

$$p\left(\mathbf{x}|\widetilde{\mathbf{Y}}\right) \propto L\left(\mathbf{x}|\widetilde{\mathbf{Y}}\right). \tag{9}$$

The Kullback-Leibler divergence (KLD) is a statistical measure for the difference between two distributions, which are in this case the prior and posterior parameter distributions of a given model parameter x_i :

$$KLD_i = \int p\left(x_i|\widetilde{\mathbf{Y}}\right) \ln\left(\frac{p\left(x_i|\widetilde{\mathbf{Y}}\right)}{p(x_i)}\right) dx_i. \tag{10}$$

For numerical computation, the posterior was discretized and normalized over the same bins as the prior to ensure comparability. Schübl et al. (2022) used the KLD to quantify the information gain from inverse estimation. A larger KLD value indicates a higher information gain, and a KLD value greater than 1 suggests that the posterior distribution is substantially different from the uniform prior distribution.

3.2.6. Convergence Diagnostics

MCMC diagnostics were used to assess whether an MCMC algorithm has successfully converged to the target posterior distribution. The acceptance rate (AR) helps assessing the efficiency and effectiveness of the sampling process, providing insights into how well the MCMC algorithm is performing. The AR is computed as the ratio of the accepted proposals, based on the Metropolis acceptance criterion, and the total number of proposals, and would optimally be between 15% and 30%, and is acceptable between 10% and 50%. A low AR (<10%) indicates that the proposals are rarely accepted. This might happen if the step size in the proposal distribution is too large, or if the algorithm is unable to find good parameter sets, for example, due to narrow priors or contradictory observations. A high AR (>50%) indicates that the majority of the proposals are accepted. This might happen if the step size is too small, leading to slow exploration of the parameter space, or if the number of observations is limited or the observations are very uncertain so that almost all parameter sets result in an acceptable model outcome.

The Gelman-Rubin multichain $\hat{R}$ statistic is a convergence criterion based on the between and within-variance of N independent chains of length $T = 2n$ and discards the first n samples in each chain, which corresponds with a 50% burn-in period. For each parameter, the variances from the last n iterations of the N chains are estimated:

$$s^2 = \frac{n-1}{n} W + \frac{1}{n} B, \tag{11}$$

19447973, 2026, 2, Downloaded from https://agupubs.onlinelibrary.wiley.com/doi/10.1029/2025WR041324 by Forschungszentrum Jülich GmbH Research Center, Wiley Online Library on [17/05/2026]. See the Terms and Conditions (https://onlinelibrary.wiley.com/terms-and-conditions) on Wiley Online Library for rules of use; OA articles are governed by the applicable Creative Commons License

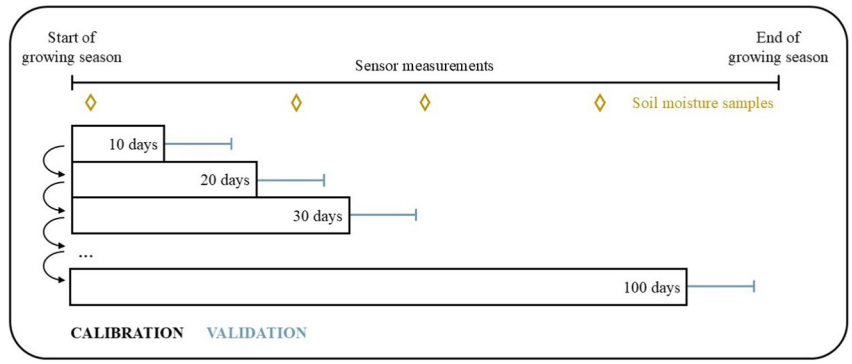

Figure 3. Schematic overview of the temporal evaluation approach to assess model performance in function of data availability in the context of real-time model application.

where B is the variance between the means from N chains, W is the average of the N within-chain variances, and s^2 is the unbiased estimate of the target variance. The convergence can be monitored by the shrink factor $\hat{R}$ which is calculated as:

$$\hat{R} = \sqrt{\frac{N+1}{N}\frac{s^2}{W} - \frac{n-1}{Nn}}, \tag{12}$$

where $\hat{R}$ values smaller than 1.2 indicate convergence (Gelman & Rubin, 1992).

3.3. Performance Evaluation

3.3.1. Temporal Evaluation Approach

In this study, model performance was evaluated temporally, that is, in function of time and data availability, mimicking the real-time application of the model (Figure 3). This approach was suggested due to expected variations in model performance depending on data availability for model calibration and lead time of predictions. For instance, after 20 days, 20 daily averaged sensor measurements and one composite soil moisture sample are available. This 20-day period is defined as the calibration period. Subsequently, soil moisture content is predicted for the next 7 days, which is defined as the validation period. In a real-time application, such 7-day forecasts would rely on weather forecasts. However, in the present study, the uncertainty due to weather prediction was intentionally excluded by using historical measured weather data for the prediction period. This allows isolating the effects of model structure and calibration data availability on soil moisture prediction performance. After 30 days, we do the same, but now with 30 days of sensor measurements and two composite soil moisture samples. This continues until the end of the cropping cycle is reached. The "end-of-cycle" calibration is defined as the model calibration using all measurement data of the full cropping cycle.

3.3.2. Evaluation Metrics

First, we evaluated whether a low-dimensional model can be accurately calibrated using samples and sensor data after applying a generalized sensor calibration, while accounting for measurement error covariance. At each 10-day time step of each cropping cycle, both the calibration and validation period were assessed using the sample-based root mean squared deviation (RMSD) by comparing the model simulations with the samples (Equation 13).

$$\mathrm{RMSD} = \sqrt{\frac{\sum_{i=1}^{n}(\theta_{\mathrm{sim},i} - \theta_{\mathrm{samp},i})^2}{n}}, \tag{13}$$

where $\theta_{\mathrm{sim},i}$ is the SWC simulated by the maximum likelihood (ML) model, $\theta_{\mathrm{samp},i}$ is the measured SWC by the samples and n is the number of days in the calibration or validation period. Since the sensor data are known to be potentially biased, a bias-corrected RMSD (bcRMSD) was calculated when comparing model simulations with in

19447973, 2026, 2, Downloaded from https://agupubs.onlinelibrary.wiley.com/doi/10.1029/2025WR041324 by Forschungszentrum Jülich GmbH Research Center, Wiley Online Library on [17/05/2026]. See the Terms and Conditions (https://onlinelibrary.wiley.com/terms-and-conditions) on Wiley Online Library for rules of use; OA articles are governed by the applicable Creative Commons License

19447973, 2026, 2, Downloaded from https://agupubs.onlinelibrary.wiley.com/doi/10.1029/2025WR041324 by Forschungszentrum Jülich GmbH Research Center, Wiley Online Library on [17/05/2026]. See the Terms and Conditions (https://onlinelibrary.wiley.com/terms-and-conditions) on Wiley Online Library for rules of use; OA articles are governed by the applicable Creative Commons License

situ sensor measurements. For this bcRMSD, the sensor bias b was calculated for each cropping cycle as the systematic deviation between the soil moisture samples $(\overline{\theta}_{\text{samp,all}})$ and the sensor data $(\overline{\theta}_{\text{sens,all}})$ over the whole cropping cycle for the given field (Equation 14).

$$\text{bcRMSD} = \sqrt{\frac{\sum_{i=1}^{n}(\theta_{\text{sim},i} - \theta_{\text{sens},i} - b)^2}{n}} \text{ with } b = \overline{\theta}_{\text{samp,all}} - \overline{\theta}_{\text{sens,all}}, \tag{14}$$

where $\theta_{\text{sens},i}$ is the average SWC measured by the three sensors. Additionally, the Nash-Sutcliffe Efficiency (NSE) is calculated using Equation 15 to evaluate the model's performance by comparing the model's residual variance to the variance of the soil moisture samples.

$$\text{NSE} = 1 - \frac{\sum_{i=1}^{n}(\theta_{\text{sim},i} - \theta_{\text{samp},i})^2}{\sum_{i=1}^{n}\left(\overline{\theta}_{\text{samp}} - \theta_{\text{samp},i}\right)^2}, \tag{15}$$

where $\overline{\theta}_{\text{samp}}$ is the average of the observations $(\theta_{\text{samp},i})$ over the n days. The bias-corrected Nash-Sutcliffe Efficiency (bcNSE) is calculated using sensor data to evaluate the model's performance after removing the sensor bias b (Equation 16).

$$\text{bcNSE} = 1 - \frac{\sum_{i=1}^{n}(\theta_{\text{sim},i} - \theta_{\text{sens},i} - b)^2}{\sum_{i=1}^{n}\left(\overline{\theta}_{\text{sens}} - \theta_{\text{sens},i}\right)^2} \text{ with } b = \overline{\theta}_{\text{samp,all}} - \overline{\theta}_{\text{sens,all}}, \tag{16}$$

where $\overline{\theta}_{\text{sens}}$ is the average of the sensor observations $(\theta_{\text{sens},i})$ over the n days.

Second, we quantified the predictive power of the model framework using differences in model performance during the calibration and validation period as a proxy. The (bias-corrected) predictive power index (PPI_{bc}) is a performance ratio of the model accuracy during validation and calibration, and is calculated using Equation 17.

$$\text{PPI}_{\text{bc}} = \frac{\text{bcRMSD}_{\text{cal}}}{\text{bcRMSD}_{\text{val}}}. \tag{17}$$

If $\text{PPI}_{\text{bc}} \approx 1$, the model has good predictive power, while a lower PPI_{bc} indicates performance degradation in the validation period, that is, lower predictive power, suggesting overfitting. In contrast, $\text{PPI}_{\text{bc}} > 1$ suggests the model unexpectedly performs better on the validation data set. This may be due to underfitting, that is, the model might not be complex enough to capture the underlying patterns in the calibration data, or due to the validation period being less representative of the full data variability. The PPI_{bc} is optimal between 0.8 and 1.2, and is unacceptable below 0.5 and over 1.5.

Finally, the sample-based RMSD and sensor-based bcRMSD can be compared to the model simulation uncertainty, which is quantified by the RMSD across the model ensemble. This is analogous to model prediction uncertainty in classical regression analysis. The model RMSD is defined as the root mean square deviation between each model ensemble simulation and the ML model simulation (Equation 18), since the ML is used as simulation reference for the sample-based RMSD and sensor-based bcRMSD.

$$\text{Model RMSD} = \sqrt{\frac{\sum_{i=1}^{n}\sum_{m=1}^{k}(\theta_{\text{ML},i} - \theta_{m,i})^2}{n \times k}}, \tag{18}$$

where k is the number of model ensemble members, $\theta_{m,i}$ is the soil moisture estimate of model ensemble member m at time step i, and $\theta_{\text{ML},i}$ is the ML soil moisture estimate.

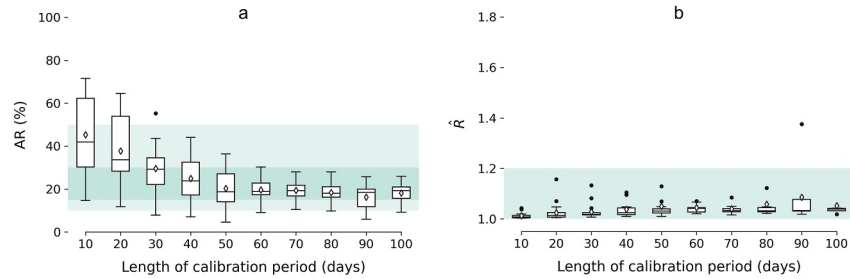

Figure 4. Acceptance rate (AR) (a) and aggregated Gelman-Rubin $\hat{R}$ statistic (b) of the 18 cropping cycles in function of the number of calibration days. The green shaded area indicates the optimal range of AR (15%–30%, acceptable between 10% and 50%) and $\hat{R}$ (<1.2).

4. Temporal Model Performance Evaluation

4.1. DREAM$_{(ZS)}$ Diagnostics

The values of the average AR in the period after 50% burn-in are summarized in boxplots in function of the amount of daily sensor data used in the inverse calibration (Figure 4a). Except for some cases with only 10 or 20 calibration days, the AR is generally between 10% and 50%, while after 40 calibration days, the majority of the cases reaches an optimal AR between 15% and 30%.

The Gelman-Rubin $\hat{R}$ statistic after 50% burn-in is required to be below 1.2 to ensure adequate convergence of the parameter estimates, both within and between chains. The $\hat{R}$ statistic was first calculated for each parameter in each case by averaging over the last 50% MCMC iterations. Then, the $\hat{R}$ values of all 12 parameters were averaged within each case, resulting in a single $\hat{R}$ value per case. These aggregated $\hat{R}$ values are summarized in boxplots in function of the amount of daily sensor data used in the inverse calibration (Figure 4b), which show good convergence.

The AR was expected to decrease with an increasing amount of calibration data, while the Gelman-Rubin $\hat{R}$ statistic was expected to increase, indicating reduced convergence efficiency. This expectation is confirmed by the observed values. As more data are used, it becomes increasingly difficult to identify parameter sets capable of reproducing longer measurement time series. Additionally, a mechanical effect of the MCMC algorithm contributes to this behavior: the likelihood function becomes more peaked with increasing data, narrowing the region of high posterior density. As a result, the Markov chains mix more poorly within a fixed number of iterations, leading to lower acceptance rates and higher $\hat{R}$ values. Although in theory MCMC chains would converge given enough iterations, in practice, more data can make convergence slower and more challenging within the same number of iterations.

These diagnostic values indicate that our relatively simple soil water balance model with 12 uncertain model parameters can be calibrated efficiently within a single cropping cycle with in situ soil moisture measurements in a Bayesian inverse modeling framework using DREAM$_{(ZS)}$.

4.2. Model Accuracy and Predictive Power

To illustrate the temporal evaluation approach and assess how well SWIM^2 reproduces and predicts SWC dynamics, Figure 5 shows the SWC measurements, and in-season simulated and observed SWC for a case study of Belgian endive in Herent (PLV) in 2023. The dotted vertical line marks the day of model calibration, separating the calibration phase on the left from the prediction and validation phase on the right. This example illustrates how model accuracy and predictive power were evaluated under real-time conditions, mimicking the operational use of the framework during the growing season.

4.2.1. Evaluation With (Biased) Sensor Data

First, the model performance was evaluated using the averaged sensor data, while the calibration itself was based on both the unbiased soil moisture samples and the sensor data. This evaluation allows for assessing how well the calibrated model reproduces the full temporal dynamics captured by the sensors, despite their known systematic

19447973, 2026, 2, Downloaded from https://agupubs.onlinelibrary.wiley.com/doi/10.1029/2025WR041324 by Forschungszentrum Jülich GmbH Research Center, Wiley Online Library on [17/05/2026]. See the Terms and Conditions (https://onlinelibrary.wiley.com/terms-and-conditions) on Wiley Online Library for rules of use; OA articles are governed by the applicable Creative Commons License

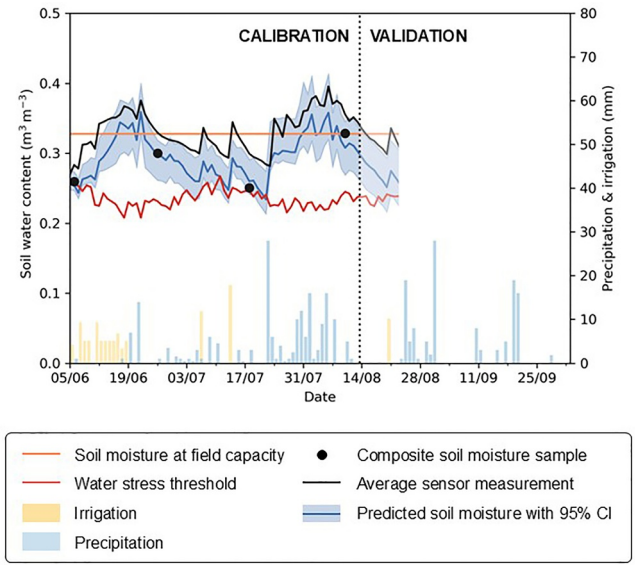

Figure 5. The in-season model output and measurements are shown for a case study of Belgian endive at PLV in Herent in 2023, 70 days into the cropping period. The blue line is the model-predicted SWC, with the 95% CI derived from the ensembles after the 50% burn-in, while the measurements are shown in black. The dotted line represents the day of model calibration, with on the left, the data that was used for model calibration. On the right of the line, SWC was predicted and validated with the corresponding measurement data.

bias. The bcRMSD values (Equation 14) of the calibration and validation period were aggregated over all case studies and are shown as boxplots in function of data availability in Figure 6a. The number of case studies that were used in the bcRMSD calculations was dependent on the amount of sensor data during the different cropping cycles and is shown in Figure 6b. The bcRMSD was generally larger during the validation period than during the calibration period, as expected. The median $bcRMSD_{cal}$ remains relatively constant as the cropping period extends and more data becomes available for calibration. The apparent decrease in $bcRMSD_{val}$ is primarily attributed to the longer case studies which have smaller errors.

The contour plot in Figure 6c represents the soil moisture simulations of the end-of-cycle calibration periods in function of the bias-corrected soil moisture measured by the sensors, with a $bcRMSD_{cal}$ of 0.0275 $m^3\ m^{-3}$ and a $bcNSE_{cal}$ of 0.867, meaning that the model explains 86.7% of the variance in the soil moisture data. The contour plot in Figure 6d represents the soil moisture predictions for all validation periods in function of the bias-corrected soil moisture measured by the sensors, with a $bcRMSD_{val}$ of 0.0396 $m^3\ m^{-3}$ and a $bcNSE_{val}$ of 0.697. When only the first four lead days are considered, $bcRMSD_{val}$ = 0.0368 $m^3\ m^{-3}$ and $bcNSE_{val}$ = 0.740. It should be noted that the performance during the validation periods, especially during the first four lead days, is only slightly lower than the performance during the end-of-cycle calibration period.

Even for a perfect model, you wouldn't expect an error smaller than the random error of the sensor measurements since the observations themselves contain uncertainty. Hence, a bcRMSD < 0.032 $m^3\ m^{-3}$ indicates that the model overfits the observations, possibly capturing noise rather than only the underlying soil moisture dynamics, which is the case for the calibration period. The limited increase in error during the validation periods suggests however that while the model may slightly overfit the data during calibration, its generalization to validation remains reasonable.

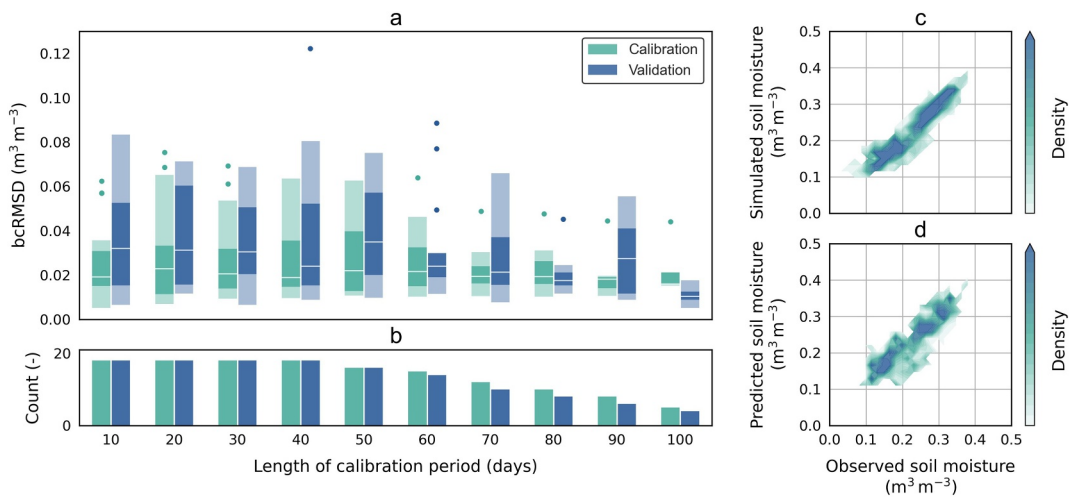

Figure 6. Boxplots of bias-corrected RMSD (bcRMSD) of the model simulation compared to the (bias-corrected) sensor data during the calibration (green) and validation (blue) period (a). Each box shows the interquartile range (IQR, 25th–75th percentile) of the data, with the median value indicated by the central line. Shaded areas beyond the central box illustrate additional spread of the data, while points indicate outliers. The number of cases is indicated by the bar plot below (b). On the right, contour plots of soil moisture values simulated with the model in function of the bias-corrected sensor measurements during the end-of-cycle calibration periods ($bcRMSD_{cal}$ = 0.0275 $m^3\ m^{-3}$ and $bcNSE_{cal}$ = 0.867) (c) and during all validation periods ($bcRMSD_{val}$ = 0.0396 $m^3\ m^{-3}$ and $bcNSE_{val}$ = 0.697) (d).

19447973, 2026, 2, Downloaded from https://agupubs.onlinelibrary.wiley.com/doi/10.1029/2025WR041324 by Forschungszentrum Jülich GmbH Research Center, Wiley Online Library on [17/05/2026]. See the Terms and Conditions (https://onlinelibrary.wiley.com/terms-and-conditions) on Wiley Online Library for rules of use; OA articles are governed by the applicable Creative Commons License

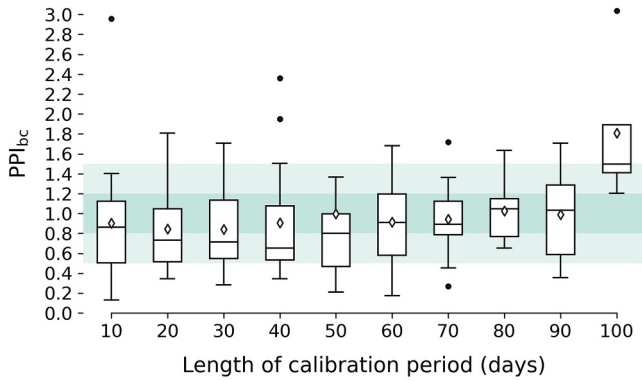

Figure 7. bcRMSD-based predictive power index (PPI_{bc}) in function of the number of calibration days. The green shaded area indicates the optimal range of PPI_{bc} (0.8–1.2, acceptable between 0.5 and 1.5).

Additionally, the $bcRMSD_{val}$ was expected to increase with increasing lead day due to error propagation, while it was expected to decrease with an increasing number of calibration days. The $bcRMSD_{val}$ was computed for each combination of calibration days and lead day resulting in a heatmap that reflects this general trend (Appendix A: Figure A1). However, temporal deviations from this pattern are also observed, which are likely influenced by soil moisture dynamics and hydrological events.

Second, the predictive power of the model was evaluated based on the ratio of the bcRMSD values during the calibration and validation period, defined as the PPI_{bc} (Equation 17), which is shown in function of data availability in Figure 7. The majority of the study cases had a PPI_{bc} between 0.5 and 1.5, while the average PPI_{bc} values were generally in the optimal range between 0.8 and 1.2. The PPI_{bc} values that are larger than 1.5 indicate unexpected high accuracy during the validation period compared to the calibration period. The extremes at both the upper and lower side could be due to very small bcRMSD values (e.g., the ratio of 0.01 and 0.025). Mind that the longer the calibration period, the less cases could be used for the computation of PPI_{bc}, for example, only four cases were considered for a calibration period of 100 days (Figure 6b).

4.2.2. Evaluation With (Unbiased) Sample Data

Next, the model performance was evaluated using the unbiased soil moisture samples, while the calibration itself was based on both these samples and the sensor data. This evaluation allows for assessing how well the calibrated model reproduces the actual soil moisture values measured by the unbiased samples. During the calibration periods, the soil moisture simulations exhibit a strong, unbiased linear relation with the soil moisture samples, with an overall $RMSD_{cal}$ of 0.0189 $m^3\ m^{-3}$ and a NSE_{cal} of 0.923. This $RMSD_{cal}$ is substantially smaller than the sensor-based $bcRMSD_{cal}$, but is notably larger than the error in the composite soil moisture samples (0.0038 $m^3\ m^{-3}$). This suggests that the deviation between the model simulations and the samples is not solely due to sample errors but also may include a model error, that is, an imperfect representation of soil moisture dynamics by the model. For example, for 80 calibration days, the sample-based $RMSD_{cal}$ was 0.024 $m^3\ m^{-3}$ while the model simulation uncertainty $RMSD_{cal}$ was 0.015 $m^3\ m^{-3}$, suggesting a (residual) model error of approximately 0.018 $m^3\ m^{-3}$ while keeping in mind the sample error of 0.0038 $m^3\ m^{-3}$. This shows that model simulation uncertainty captures part of the model error due to parameter uncertainty but does not account for structural model errors. It is also important to note that the sensor data used in the calibration also impact the deviation between the model simulations and the samples. The high NSE_{cal} indicates that the model still explains most of the variance in the soil moisture sample data, indicating good overall performance despite the remaining model error.

Figure 8a shows the $RMSD_{cal}$ as a function of the number of calibration days, indicating an increase in $RMSD_{cal}$ with an increasing average number of samples during this calibration period. This trend occurs because it becomes increasingly more challenging to identify parameter sets that align well with an increasing number of samples.

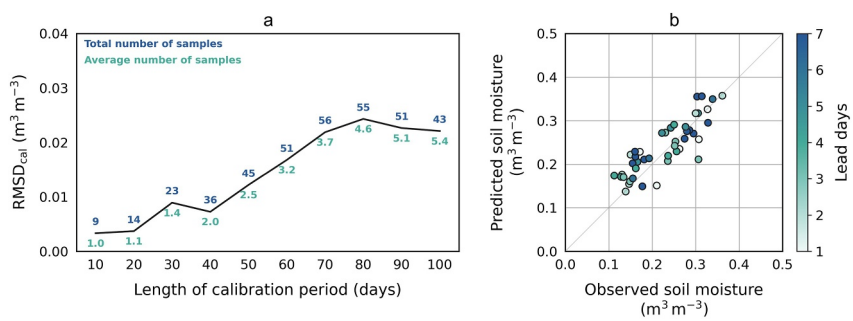

Figure 8. Sample-based RMSD during the calibration period, in function of number of calibration days (a), and the model simulation compared to the soil moisture samples during the validation period, plotted in function of the lead day ($RMSD_{val}$ = 0.0383 $m^3\ m^{-3}$ and NSE_{val} = 0.695) (b).

19447973, 2026, 2, Downloaded from https://agupubs.onlinelibrary.wiley.com/doi/10.1029/2025WR041324 by Forschungszentrum Jülich GmbH Research Center, Wiley Online Library on [17/05/2026]. See the Terms and Conditions (https://onlinelibrary.wiley.com/terms-and-conditions) on Wiley Online Library for rules of use; OA articles are governed by the applicable Creative Commons License

19447973, 2026, 2, Downloaded from https://agupubs.onlinelibrary.wiley.com/doi/10.1029/2025WR041324 by Forschungszentrum Jülich GmbH Research Center, Wiley Online Library on [17/05/2026]. See the Terms and Conditions (https://onlinelibrary.wiley.com/terms-and-conditions) on Wiley Online Library for rules of use; OA articles are governed by the applicable Creative Commons License

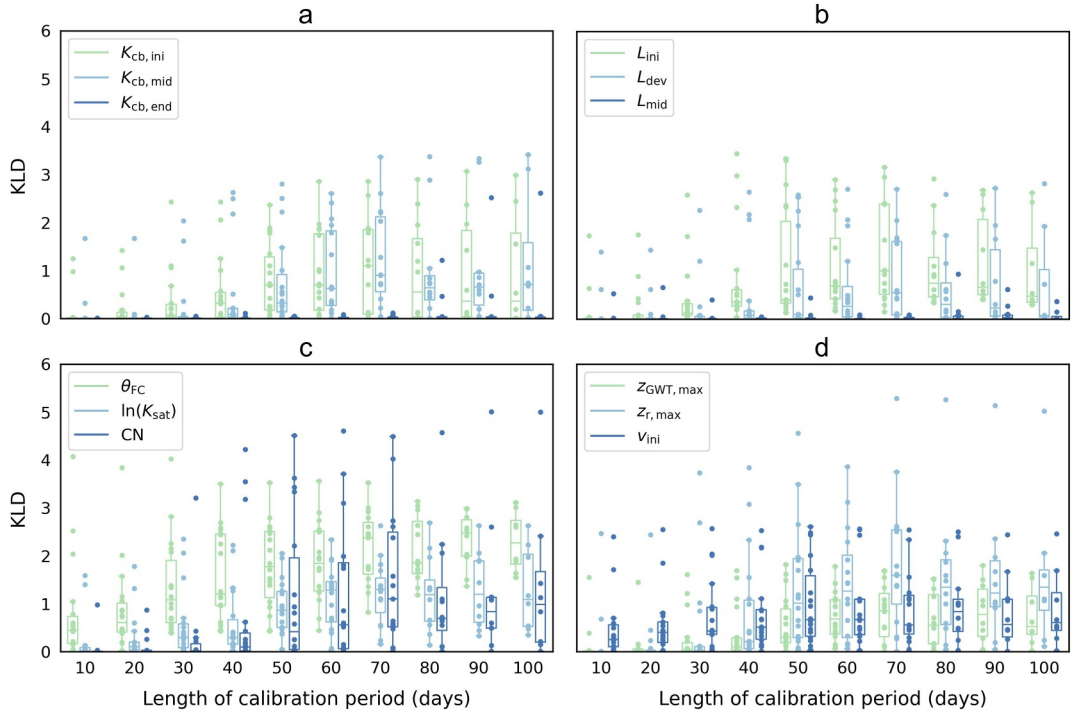

Figure 9. Evolution of the Kullback-Leibler divergence (KLD), as an indication of information gain, for parameters describing crop canopy (a), crop growth stages (b), soil hydraulic properties (c), and initial and boundary parameters (d).

When only one or two samples are used in the calibration period, the model can fit those samples very tightly, possibly even memorizing noise, leading to a low $RMSD_{cal}$ (≈0.005 m^3 m^{-3}) that closely matches the sample error (0.0038 m^3 m^{-3}). However, this model fit does not generalize well over the remaining period of the growing season. As more samples are included in the calibration, for example, four or five, the model has to account for more variation and becomes less tightly fit to each individual sample. This results in an increased $RMSD_{cal}$, even though this is the better, more generalizable, and less overfit model. Once a sufficient number of observations have been used in the model calibration, the model reaches a point where it has effectively learned the full range of soil moisture states and is not fitting noise. From that moment on, $RMSD_{cal}$ stabilizes with an increasing number of calibration data. However, the limited number of samples during the calibration periods do not allow us to confirm this trend. Also, since the calibrated model output is influenced by both sensor data and samples, accounting for the increasing number of samples and its effect on $RMSD_{cal}$ is not straightforward.

A slightly larger error was observed when the soil moisture predictions were compared to the soil moisture samples during the validation periods of all calibration periods (Figure 8b), with an overall $RMSD_{val}$ of 0.0383 m^3 m^{-3}, and a NSE of 0.695. Since the number of samples during the validation periods were limited and randomly distributed over this period, we cannot make any statement about differences between lead days based on the samples alone.

4.3. Posterior Parameter Distributions

The information gain from the inverse estimation of the model parameters from prior to posterior distribution was quantified by the KLD, which is expected to increase with an increasing amount of calibration data. For most of the model parameters, this expected increase was observed (Figure 9). However, since the prior distribution is always defined as the initial uniform distribution and is not updated with the previous posterior distribution, the KLD may decrease when additional, potentially contradictory observations are included in the calibration. Since some of the model parameters are growth stage dependent, their information gain is expected to increase only once the corresponding stage of the growing period is reached. For example, crop parameters of the initial stage ($K_{cb,ini}$ and L_{ini}) showed an increase in KLD early in the cropping cycle, while crop parameters of the vegetative stages only gained information after 40 ($K_{cb,mid}$ and L_{dev}) or 80 ($K_{cb,end}$ and L_{mid}) calibration days. On top of this,

19447973, 2026, 2, Downloaded from https://agupubs.onlinelibrary.wiley.com/doi/10.1029/2025WR041324 by Forschungszentrum Jülich GmbH Research Center, Wiley Online Library on [17/05/2026]. See the Terms and Conditions (https://onlinelibrary.wiley.com/terms-and-conditions) on Wiley Online Library for rules of use; OA articles are governed by the applicable Creative Commons License

most vegetable cropping cycles do not include a senescence stage, which is why the KLD never increased for these cases. A similar reasoning applies to parameters that are dependent on hydrological events such as heavy precipitation or strong drying of the soil (e.g., θ_{FC}, CN and K_{cb} parameters), and thus need such events to gain information.

The overall sensitivity of all parameters based on KLD, from lowest to highest, follows the order: $K_{cb,end} < L_{mid} < L_{dev} < K_{cb,ini} < \theta_{ini} < z_{GWT,max} < K_{cb,mid} < L_{ini} < CN < \ln(K_{sat}) < z_{r,max} < \theta_{FC}$. The stabilized median KLD of L_{dev}, $K_{cb,ini}$, θ_{ini}, $z_{GWT,max}$, $K_{cb,mid}$, L_{ini} and CN were between 0.1 and 1 (Figure 9), suggesting that the posterior distributions were overall not substantially different from the uniform prior distributions. However, KLD exceeded 1 for these parameters in individual case studies, illustrating parameter importance and sensitivity under specific conditions. In contrast, the stabilized median KLD of $\ln(K_{sat})$, $z_{r,max}$ and θ_{FC} exceeded 1, suggesting that their posterior distributions were generally substantially different from their uniform priors. This indicates that the model is most sensitive to these parameters under most conditions, and uncertainties in their values would have the largest impact on model predictions. These three parameters have a direct impact on the soil water balance, with $\ln(K_{sat})$ being the main driver of capillary rise, regulating water movement from the groundwater to the root zone and directly influencing SWC, while θ_{FC} determines the upper limit of plant-available water after excess drainage has occurred. $z_{r,max}$ is a key driver of root growth and plant water availability, as it determines the depth from which roots can extract water, directly linking available water to soil moisture content which is the model state used for calibration. A larger $z_{r,max}$ leads to more water addition from layers at FC below the root zone. Additionally, the model appears insensitive to crop parameters associated with later growth stages ($K_{cb,end}$ and L_{mid}), as their KLD values remain very low. This suggests that excluding them from calibration would not affect model performance. However, they are still included to maintain a generalizable framework that can be applied to other crop types where these parameters might be more relevant.

Correlations among the posterior distributions across all case studies provide insight into parameter dependencies and potential redundancies in the model and its calibration. Spearman correlations were used to assess non-linear relationships among posterior parameters, capturing consistent increases or decreases regardless of functional form, whereas Pearson correlations quantify linear relationships. This distinction explains why some parameter pairs show moderate linear correlations but weak rank-based correlations. Strong correlations suggest that certain parameters are inherently linked, meaning that changes in one may systematically influence another. Almost all correlations were lower than 0.5, indicating that most parameters exhibit relatively weak dependencies, allowing for independent parameter estimation. However, a few notable correlations suggest underlying process interactions. θ_{FC} exhibited a strong positive Spearman correlation (>0.4) with θ_{ini}, which may be due to wet conditions at the start of the cropping cycles. CN showed strong positive Pearson correlations with $z_{GWT,max}$, L_{ini} and L_{mid}. Furthermore, $\ln(K_{sat})$ had a strong negative Pearson correlation with $K_{cb,mid}$, while $z_{GWT,max}$ had a strong negative Pearson correlation with θ_{ini}. The full correlation matrices can be found in Appendix A: Figures A2–A3. While $z_{r,max}$ didn't show significant correlations across the case studies, it often exhibited strong negative Pearson correlations with CN and θ_{FC} on a case-by-case basis. Since both $z_{GWT,max}$ and $\ln(K_{sat})$ are drivers of capillary rise, a strong positive correlation was expected, but only moderate correlations were observed in some individual cases.

When comparing the end-of-cycle parameter estimates of θ_{FC} with measured soil properties, a negative Spearman correlation of −0.45 (Pearson correlation of −0.33) was found between the measured BD and the estimated θ_{FC} across all fields, while a positive Spearman correlation of 0.54 (Pearson correlation of 0.64) was found between the measured SWC at pF 2 and the estimated FC (Figures A2–A4). These results indicate that the θ_{FC} estimates are realistic and physically consistent rather than arbitrary or compensating for model shortcomings.

5. Impact of In Situ Measurements and Observational Errors

5.1. Model Framework Scenarios

The temporal evaluation of model performance (Section 4) was conducted on the reference model scenario, that is, using both the sensor data and the uncorrelated soil moisture samples to calibrate the model parameters in $DREAM_{(ZS)}$ while applying the pooled error covariance matrix. Six additional scenarios are presented here to assess the impact of two types of SWC measurements and their error covariance on the model calibration precision and accuracy (Table 2).

19447973, 2026, 2, Downloaded from https://agupubs.onlinelibrary.wiley.com/doi/10.1029/2025WR041324 by Forschungszentrum Jülich GmbH Research Center, Wiley Online Library on [17/05/2026]. See the Terms and Conditions (https://onlinelibrary.wiley.com/terms-and-conditions) on Wiley Online Library for rules of use; OA articles are governed by the applicable Creative Commons License

Table 2
Model Scenarios to Assess the Impact of SWC Measurements and Their Sensor Error Covariance

Scenario	$DREAM_{(ZS)}$ observations	Sensor measurement error covariance
Reference	Sensor + samples	Pooled
A	Sensor only	Pooled
B	Sensor only	Zero
C	Sensor + 2 samples	Pooled
D	Samples only	–
E	Sensor + samples	Zero
F	Sensor + samples	Estimated

Both scenario A and B use only sensor data to calibrate the model parameters in $DREAM_{(ZS)}$. This means that no independent, unbiased measurements are available to correct for possible sensor bias. While scenario A does consider sensor measurement error covariance to account for this possible sensor bias, scenario B does not and assumes zero error covariance. Scenario A and B are both expected to produce a SWB model, that is, biased compared to the (unbiased) samples with a deviation, that is, similar to the sensor bias. The uncertainty estimates for the two scenarios will, however, differ, as scenario A accounts for error covariance, leading to wider posterior distributions and higher uncertainty estimates compared to scenario B.

Scenario C uses only the first two soil moisture samples in addition to the sensor data to calibrate the model parameters. This scenario will be used to assess the necessity of periodic samples during the cropping cycle. In contrast to scenarios A to C, scenario D uses only the independent, unbiased soil moisture samples. Since the samples are roughly taken on a two-weekly basis, the samples do not contain information on daily soil moisture dynamics, which is expected to result in an unbiased, but uncertain SWB model.

Scenario E uses both sensor data and the soil moisture samples, like the reference scenario, but assumes zero measurement error covariance. This is expected to produce a model, that is, biased compared to both the (unbiased) samples and the (biased) sensor, depending on the weight of samples versus sensor data.

Finally, in scenario F, sensor error variance and error autocorrelation are estimated in $DREAM_{(ZS)}$ as an alternative to using the pooled error covariance matrix. In this approach, the error variance is assumed constant and is estimated on a logarithmic scale (between 0.00001 and 1). Error autocorrelation is also assumed constant and is estimated from a uniform prior between 0 and 1.

The differences between the scenarios and the impact of the in situ measurements on model calibration are discussed in this section. The reference scenario and the additional six scenarios (A-F) are illustrated in Figure 10, where the end-of-cycle SWC simulation, that is, calibrated with and simulated for the full growth period, is shown for a case study of Belgian endive at PLV in Herent in 2023, for each of the scenarios. In this case study, the sensor data were biased compared to the soil moisture samples. This figure illustrates the effect of the model calibration scenarios for a single case and serves as a visual reference for understanding the general effects of the different scenarios across all cases. The full case study output can be found in Text S2 of Supporting Information S1.

5.2. Added Value of Independent Soil Moisture Samples

Scenario A uses only sensor data to calibrate the model parameters in $DREAM_{(ZS)}$. The sample-based $RMSD_{cal}$, which is plotted versus the number of calibration days in Figure 11b, is consistently higher for scenario A compared to the reference scenario with a difference similar to the systematic sensor error standard deviation of 0.033 $m^3\ m^{-3}$. This difference is a reflection of the bias that exists between the samples and the sensor data. It is important to take note here that the RMSD represents the accuracy of the ML soil moisture simulation. To know whether this scenario may reflect the true soil moisture status, the simulated soil moisture uncertainty needs to be considered as well. Soil moisture uncertainty estimates during the calibration period are much larger when only (biased) sensor data are used, compared to the reference scenario where samples are included (Figure 11a), which is clearly illustrated by the case study in Figure 10. This is also reflected in the KLD values, which were generally lower than 1 for all model parameters (not shown), indicating that, for scenario A, the posterior distributions were

10.1029/2025WR041324

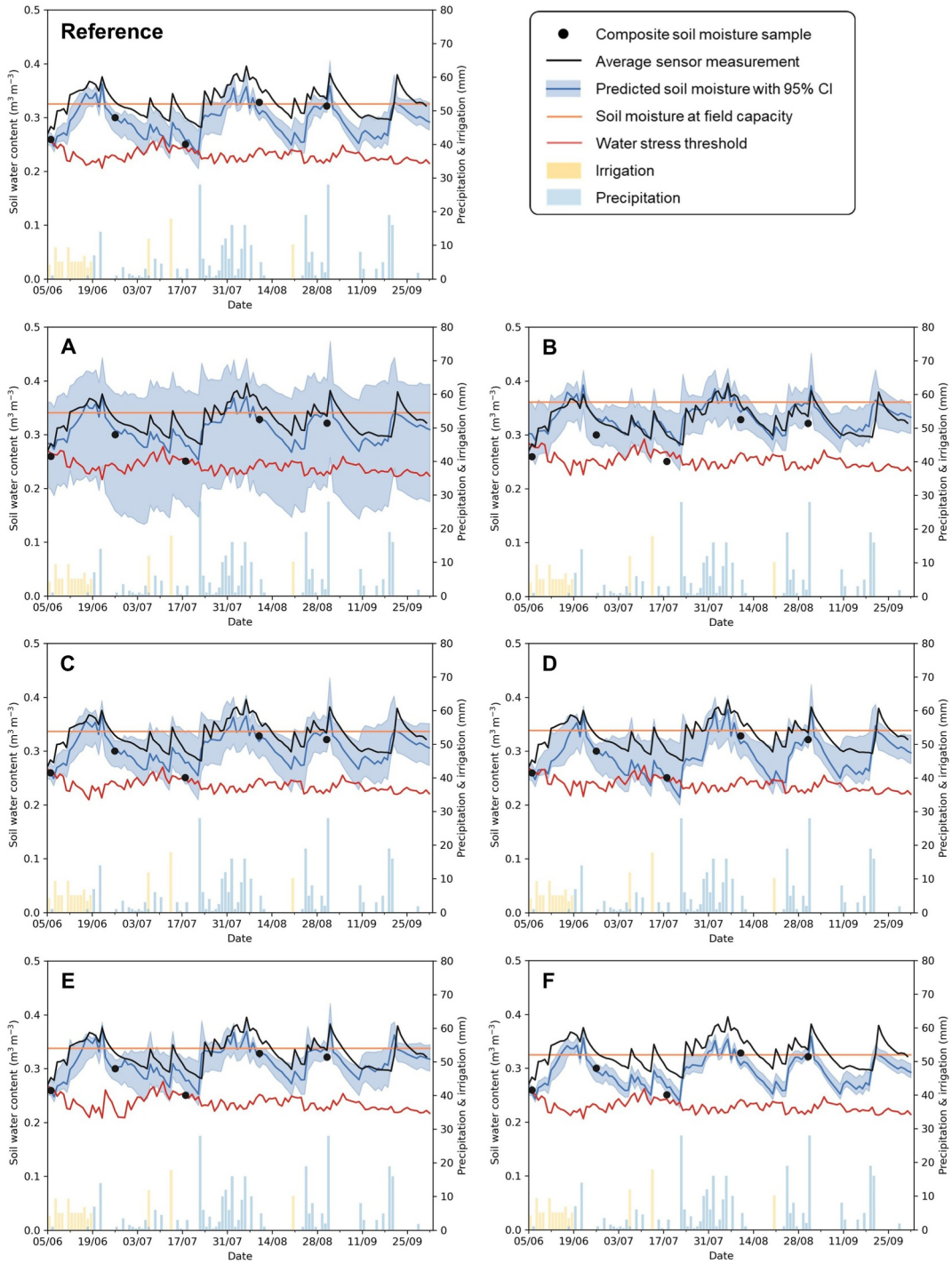

Figure 10. The end-of-cycle model output and measurements are shown for a case study of Belgian endive at PLV in Herent in 2023. The blue line is the model-predicted SWC, with the 95% CI derived from the ensembles after the 50% burn-in, while the measurements are shown in black. The reference scenario where samples and sensor data with the pooled covariance are used in the calibration is compared to scenarios (a) using sensor data only with the pooled error covariance, (b) using sensor data only and assuming zero covariance, (c) using sensor data and the first two samples, (d) using samples only, (e) using samples and sensor data assuming zero covariance, (f) using samples and sensor data while estimating the measurement error covariance matrix (see Table 2).

19447973, 2026, 2, Downloaded from https://agupubs.onlinelibrary.wiley.com/doi/10.1029/2025WR041324 by Forschungszentrum Jülich GmbH Research Center, Wiley Online Library on [17/05/2026]. See the Terms and Conditions (https://onlinelibrary.wiley.com/terms-and-conditions) on Wiley Online Library for rules of use; OA articles are governed by the applicable Creative Commons License

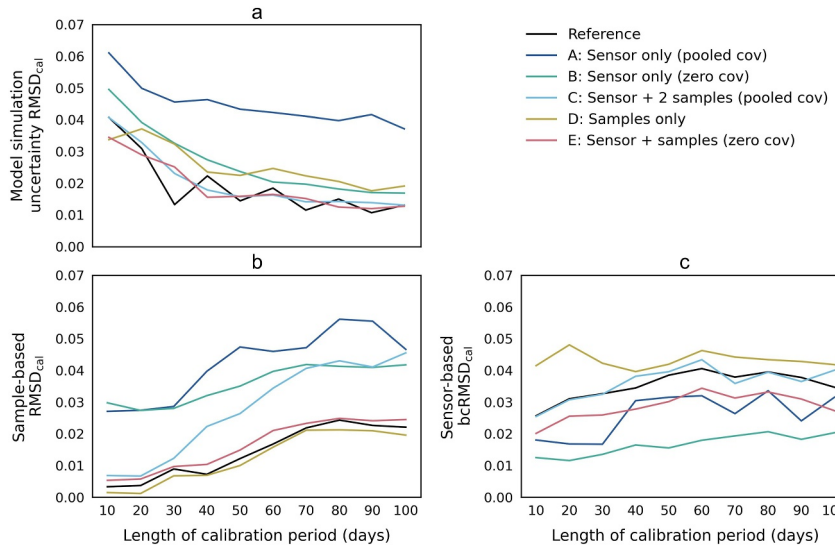

Figure 11. Model RMSD representing model simulation uncertainty (a), sample-based RMSD (b), and sensor-based bcRMSD (c) during the calibration period, shown for the reference scenario compared to scenarios A-E in function of number of calibration days.

not substantially different from the uniform priors. In summary, when random and systematic sensor errors are taken into account correctly, using only (biased) sensor data will result in an unprecise soil moisture simulation and prediction with an uncertainty range that includes the true SWC. These results suggest that independent soil moisture samples are required to correct for sensor bias, to calibrate the model parameters more efficiently, and to obtain more precise parameter and soil moisture estimates.

Scenario C uses the first two samples in addition to the sensor data to calibrate the model parameters in DREAM$_{(ZS)}$. For this scenario, only 7 study cases with more than 90 calibration days and more than 4 soil moisture samples were used to compare soil moisture accuracy with the reference scenario, and only the end-of-cycle simulation was considered. The RMSD of the model simulation compared to the first two samples and the model simulation compared to the remaining three to five samples per case that were not used in the inverse estimation are shown in Figure 12. The deviation of the model simulation compared to the first two samples was similar compared to the reference scenario, as expected. In contrast, the deviation of the model simulation compared to the remaining samples was significantly larger, with an RMSD of 0.056 m^3 m^{-3} in scenario C compared to an RMSD of 0.025 m^3 m^{-3} in the reference scenario (Figure 12). This RMSD is similar to the RMSD in scenario A where no samples were used, indicating that the first two samples contribute little or even negatively to the model performance for the remaining part of the cropping cycle.

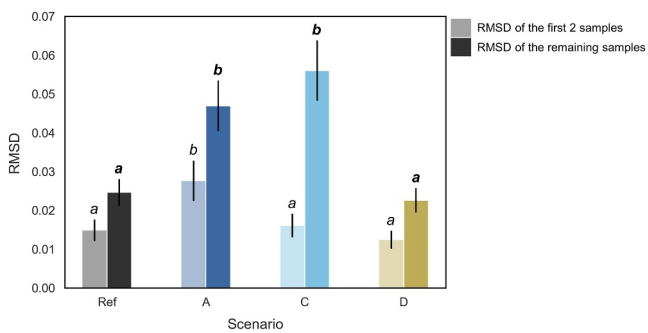

Figure 12. Sample-based RMSD of the first two samples and the remaining samples after the first two, for the different scenarios. The reference scenario (Ref) where samples and sensor data with the pooled covariance are used in the calibration is compared to scenarios A: using sensor data only with the pooled error covariance, C: using sensor data and the first two samples, D: using samples only (see Table 2). The error bars, representing the standard error, and letters indicate significant differences in RMSD between the scenarios. For this analysis, only 7 cases with more than 90 calibration days and more than 4 soil moisture samples were used, and only the end-of-cycle simulation was considered.

The large RMSD after the first two samples in scenario C may be attributed to several factors. First of all, the biased sensor data regains the upper hand in terms of weight during the remaining period after the first two samples. Second, errors could arise in the early samples due to challenges in accurately measuring wet soil conditions. Another possible reason is the reduced representativeness of the first two samples for the entire cropping cycle, as they may not adequately account for temporal variability or evolving field conditions, such as root growth or soil hydraulic property changes (e.g., soil settling or compaction). Hence, using only the early samples during calibration might introduce biases, reducing the model's ability to accurately simulate soil moisture for the remainder of the cropping cycle.

19447973, 2026, 2, Downloaded from https://agupubs.onlinelibrary.wiley.com/doi/10.1029/2025WR041324 by Forschungszentrum Jülich GmbH Research Center, Wiley Online Library on [17/05/2026]. See the Terms and Conditions (https://onlinelibrary.wiley.com/terms-and-conditions) on Wiley Online Library for rules of use; OA articles are governed by the applicable Creative Commons License

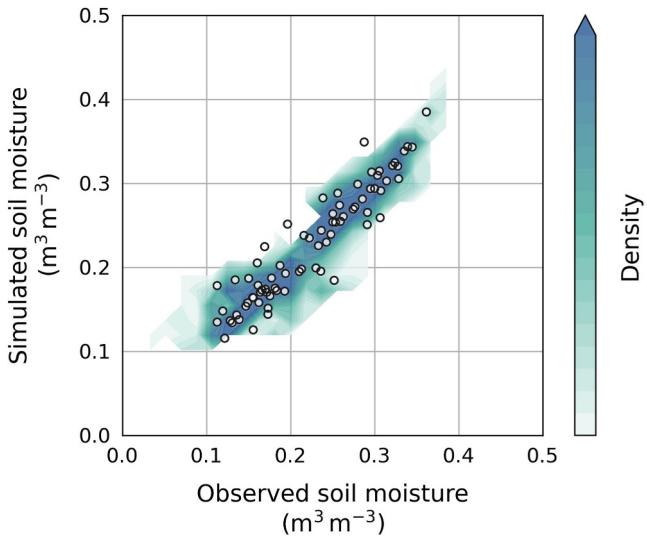

Figure 13. Contour plot of soil moisture values simulated with the model (scenario F) in function of the bias-corrected sensor measurements during the end-of-cycle calibration periods ($bcRMSD_{cal}$ = 0.0278 m^3 m^{-3} and $bcNSE_{cal}$ = 0.855), with a scatter plot in function of the soil moisture sample observations ($RMSD_{cal}$ = 0.0244 m^3 m^{-3} and NSE_{cal} = 0.872).

5.3. Added Value of Continuous Sensor Data

When calibrating model parameters in $DREAM_{(ZS)}$ using only soil moisture samples (scenario D), the resulting model simulation uncertainty during the calibration period was only slightly higher than in the reference scenario (Figure 11a) while the sensor-based accuracy of the ML soil moisture estimates was slightly reduced compared to the reference (Figure 11c). Notably, model simulation uncertainty in scenario D was especially elevated at times when no samples were available (Figure 10). This suggests that parameters influencing the temporal dynamics of soil moisture are more difficult to constrain without continuous sensor data, whereas parameters controlling systematic shifts, such as FC and initial SWC, remained largely unaffected. Moreover, estimated parameter correlations were generally weaker from those in the reference scenario.

5.4. Importance of Measurement Error Covariance

The sensor measurements may be biased compared to the soil moisture samples, which represent ground-truth. A bias corresponds to sensor observational errors that are continuously correlated over time, which is taken into account in the error covariance matrix. Neglecting this error autocorrelation results in biased model simulations and underestimated uncertainties.

Like scenario A, scenario B uses only sensor data to calibrate the model parameters, but does not correctly take into account systematic sensor observational errors. The large sample-based RMSD is similar to scenario A, but now soil moisture uncertainty estimates are much smaller than in scenario A and more similar to the reference soil moisture uncertainties (Figure 11). Consequently, the soil moisture simulations and predictions seem precise but are inaccurate when the sensor data are biased compared to the samples with an underestimated uncertainty range, that is, unable to describe the true SWC.

When using both sensor and sample data while assuming zero error covariance (scenario E), the impact of each data source depends on its total error variance. On average, one unbiased sample was available per 17 days of sensor data. Knowing that the total sensor error was only 12 times the sample error (σ_{samp} = 0.0038 m^3 m^{-3}, while σ_{tot} = 0.045 m^3 m^{-3}), the sensor data had on average the largest impact on the inverse calibration (on average a factor 1.4). Since the sensor data now has a larger impact than in the reference scenario, where error covariance is considered, the sample-based RMSD is slightly larger (Figure 11b) and the sensor-based bcRMSD is slightly smaller (Figure 11c), while soil moisture uncertainty estimates are similar in scenario E compared to the reference scenario (Figure 11a), overestimating the precision of the predictions due to a false sense of sensor accuracy.

5.5. Estimating Error (Co)Variances in DREAM

In scenario F, we extended the parameter estimation framework to include two additional parameters, that is, the sensor error variance ($\ln(\sigma^2)$) and the sensor error autocorrelation (ACOR), instead of applying the pooled error covariance matrix, allowing for a more site-specific approach to error characterization. The use of independent soil samples in the estimation process makes it possible to jointly estimate σ^2 and ACOR as they give an indication on the sensor bias, allowing for the reconstruction of the entire sensor error covariance matrix. Scenario F is illustrated by the case study in Figure 10.

The simulated soil moisture values maintained a strong agreement with both the soil moisture samples and the sensor data trends (Figure 13). The $bcRMSD_{cal}$ of the model simulation compared to the (bias-corrected) sensor data was 0.0278 m^3 m^{-3} ($bcNSE_{cal}$ of 0.855), indicating that the model effectively mimics soil moisture dynamics. This accuracy is very similar to that of the reference scenario. Furthermore, the agreement with independent soil moisture samples ($RMSD_{cal}$ of 0.0244 m^3 m^{-3} and NSE_{cal} of 0.872) suggests that the method successfully integrates the two data sources while maintaining high predictive performance.

19447973, 2026, 2, Downloaded from https://agupubs.onlinelibrary.wiley.com/doi/10.1029/2025WR041324 by Forschungszentrum Jülich GmbH Research Center, Wiley Online Library on [17/05/2026]. See the Terms and Conditions (https://onlinelibrary.wiley.com/terms-and-conditions) on Wiley Online Library for rules of use; OA articles are governed by the applicable Creative Commons License

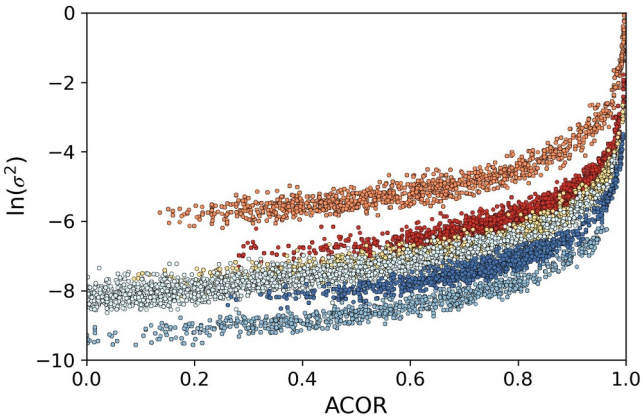

Figure 14. Posterior estimates of ACOR and $\ln(\sigma^2)$ for six case studies (shown as six colors) in 2023 to illustrate the inverse hyperbolic relation between ACOR and Var.

Moreover, the results indicate that this extended framework provides realistic estimates of σ^2 and ACOR, which align well with the pooled error model estimates. The overall average posterior ACOR value was 0.62, which is slightly larger compared to the pooled ACOR of 0.52, while σ posterior estimates were on average 0.056 $m^3\ m^{-3}$, which is slightly larger than the pooled total error $\sigma_{\overline{tot}} = 0.045\ m^3\ m^{-3}$. The larger ACOR estimates in combination with the larger error variance estimates result in a random error, that is, similar to the pooled random error, while the systematic error estimate is larger compared to the pooled systematic error. Notably, both σ^2 and ACOR exhibited considerable variation within cases, indicating strong parameter dependencies and possible equifinality (Figure 14), as well as across cases, highlighting substantial field-to-field differences. Additionally, the case-specific error covariances were derived from the ML estimates of ACOR and $\ln(\sigma^2)$, and showed a good correlation (Pearson R = 0.68) with the true sensor biases, derived from the deviation between sensor and sample data. This suggests that the inverse modeling framework can successfully and realistically identify and incorporate systematic sensor errors into the error covariance matrix.

When accounting for a systematic deviation between soil moisture samples taken infrequently and with known variance, and sensor data collected more frequently but with unknown variance, we can consider two equally likely explanatory cases. In the first case, the deviation is attributed to a systematic bias in the sensor data, resulting in a high covariance, high ACOR, and a large variance of the sensor measurement errors. In the second case, the deviation is interpreted as an unlikely random difference between the sensor and sample data, which becomes negligible compared to the high likelihood of a close fit between the model and the large volume of sensor data. In other words, the model favors the sensor data, assuming they have low variance and minimal bias, characterized by a low error ACOR. This is supported by the posterior estimates of ACOR and $\ln(\sigma^2)$, shown in Figure 14 for six case studies in 2023, which reveal an inverse hyperbolic relationship between ACOR and σ^2. In a numerical experiment (Appendix C), we assessed the theoretical relation between error variance, ACOR and LL, and found that the inverse hyperbolic relation that was observed between estimates of ACOR and Var can be attributed to the properties of the LL function being maximized. Additionally, we found that larger biases decrease the likelihood of observing a low ACOR combined with low variance, which is illustrated by the orange case in Figure 14.

Despite its advantages, the extended framework introduces a computational trade-off. The inclusion of two additional parameters increases the complexity of the inverse modeling, requiring more iterations to reach convergence and resulting in longer run times. Nevertheless, when the measurement error structure is unknown, this approach offers a valuable solution, provided that at least one unbiased data source is available, such as the soil moisture samples used in this study.

6. General Discussion and Outlook

6.1. Predicting Soil Moisture With SWIM^2

Overall, the results, obtained from 18 different cropping cycles of vegetables spread over three growing seasons and different soil textures in Flanders, demonstrate that SWIM^2 is a framework in which a low-dimensional model can be effectively calibrated using in situ measurements in real time. The framework can simulate and predict soil moisture for the next 7 days with an accuracy of 0.04 $m^3\ m^{-3}$ which is similar to the accuracy of the soil moisture sensors, which suggests that the model has a high predictive power and robustness. The slight accuracy decrease of 0.01 $m^3\ m^{-3}$ during the first four lead days compared to the calibration period substantiates this, but may indicate possible overfitting.

SWIM^2 was developed as a DSS for individual farmers to avoid water stress in high-value vegetable crops and to decide when and how much supplementary irrigation is necessary, and this in an area where water is often scarce in the periods when irrigation is needed (e.g., due to individual water extraction permits with a limited volume per year, or (regional) restrictions on surface water use in dry periods). This is why this real-time approach is

19447973, 2026, 2, Downloaded from https://agupubs.onlinelibrary.wiley.com/doi/10.1029/2025WR041324 by Forschungszentrum Jülich GmbH Research Center, Wiley Online Library on [17/05/2026]. See the Terms and Conditions (https://onlinelibrary.wiley.com/terms-and-conditions) on Wiley Online Library for rules of use; OA articles are governed by the applicable Creative Commons License

19447973, 2026, 2, Downloaded from https://agupubs.onlinelibrary.wiley.com/doi/10.1029/2025WR041324 by Forschungszentrum Jülich GmbH Research Center, Wiley Online Library on [17/05/2026]. See the Terms and Conditions (https://onlinelibrary.wiley.com/terms-and-conditions) on Wiley Online Library for rules of use; OA articles are governed by the applicable Creative Commons License

important, having the ability to forecast soil moisture for the next few days with confidence intervals. This is also why the framework was validated in a temporal assessment mimicking the real-time application of the framework (Section 3.3.1). Since soil moisture predictions showed a substantial increase in precision during the first 20 calibration days, which was shown in Figure 11a, the framework can be used for real time SWC predictions when at least 20 days of SWC sensor data are available in the growing season.

Mind that the framework, and coupled SWB model, was developed and validated for shallow-rooted vegetable crops, where groundwater depth has limited influence on root development, and was not tested for cereals, perennial crops, or phreatophytic species such as alfalfa. Root distribution functions are more relevant for deep-rooted crops and for Richards' equation–based or multi-layered models, which would introduce additional parameters beyond the current scope. It is also acknowledged that drainage may be represented too simplistically in the current model, as suggested by the relatively fast decline of simulated soil moisture after rainfall or irrigation compared to measurements. This limitation is inherent to the simple bucket-type approach, which assumes rapid drainage to field capacity. The framework could therefore be further developed and re-evaluated for different crop types, heavier clay soils, or more detailed process representations.

One of the main advantages of the framework is its minimal data requirement, making it practical and applicable for a wide range of conditions. Firstly, it does not rely on prior knowledge of soil properties, groundwater depth, or crop growth, which are often difficult or costly to obtain. Secondly, a simple setup of three sensors within a measurement zone of 80 m^2 is sufficient to monitor soil moisture, provided that potential bias is accounted for in the measurement error covariance matrix, and the soil is periodically sampled to obtain unbiased SWC measurements. Thirdly, the framework can operate effectively with limited calibration data, as demonstrated by its robust performance even in cases with fewer than 20 days of soil moisture measurements where uncertainty is large. This combination of low data dependency and adaptability makes the framework particularly suitable for deployment in commercial agricultural fields.

The use of bounded non-informative priors which only define lower and upper limits for the parameters, as was applied in $SWIM^2$, is beneficial in practical applications. Van Dongen (2006) argues that complete non-informative priors should not be used and prior knowledge should rely on common sense. The accuracy of models estimated using informative priors is previously shown to be higher than those using non-informative priors (Grzenda, 2016). Similarly, Scharnagl et al. (2011) explored the impact of three different prior distributions on Bayesian inverse modeling of in situ soil moisture observations, comparing a non-informative uniform multivariate prior with two multivariate normal prior distributions, one of which incorporates parameter correlations. Their findings showed that incorporating prior information about soil hydraulic properties significantly reduced uncertainty in parameter estimates, with the approach being both most effective and robust when the parameter correlation structure was included, and remaining reliable even when the prior information was biased. In contrast to these insights, the results of our study demonstrate that accurate and efficient parameter estimation is still achievable using non-informative priors, highlighting the adaptability and strength of the proposed framework. The use of informative priors in $SWIM^2$, for example, based on the posterior distribution of the previous growing season at that location, would however be especially beneficial during the initial phase of the cropping cycle as it could substantially improve performance when a limited amount of calibration data is available.

The uncertainty estimates of the model parameters, as well as the simulated SWC uncertainty, generally align with the observed variability of SWC in the field. This suggests that the model effectively captures the dynamics of soil moisture within the measurement zone, along with the observational errors. This enhances the reliability of its predictions for practical applications, such as irrigation scheduling or water resource management.

In this context, the choice of the $DREAM_{(ZS)}$ algorithm was motivated by the need to not only identify optimal parameter sets but to fully characterize their posterior distributions and associated uncertainties. Unlike deterministic or optimization-based algorithms (e.g., PaDDS; Asadzadeh & Tolson, 2013), $DREAM_{(ZS)}$ employs a Differential Evolution MCMC approach that efficiently explores high-dimensional, multi-modal parameter spaces. This makes it particularly suitable for uncertainty-aware hydrological modeling, where the full posterior distribution is essential to propagate parameter uncertainty into predictive soil moisture estimates.

6.2. Impact of In Situ Measurements

Since soil moisture samples are labor intensive, it is important to assess the necessity of the samples in the SWIM^2 framework. Our results show that calibrating the model using only sensor data (scenario A and B) results in a higher sample-based RMSD compared to the reference scenario, which reflects the bias between sensor data and soil moisture samples that propagates into the model. These findings underscore the importance of incorporating independent soil moisture samples to correct for sensor bias and improve model calibration and precision, which aligns with previous studies (Mane et al., 2024). Moreover, our results show that periodic soil moisture samples are required during the whole cropping cycle since two samples during the first weeks of the cropping cycle are not sufficient to correct for sensor bias during the remaining period without samples (scenario C). This can be explained by the increasing weight of the sensor data as the cropping cycle advances. Additionally, different parameters play key roles at various stages of the cropping cycle, meaning that the estimation of these parameters is influenced in different ways by the samples at different times.

Vice versa, when only periodic, unbiased samples are used in the inverse modeling framework (scenario D), the model was unbiased but lower accuracy was observed during periods without samples since soil moisture dynamics were not captured by the observations so that model parameters that describe the soil moisture dynamics cannot be calibrated with high precision. Hence, continuous sensor data are essential for capturing soil moisture dynamics and accurately estimating the corresponding model parameters.

Previous studies indicate that incorporating a multi-objective (MO) approach using multiple data types simultaneously in the likelihood function is preferred for accurately characterizing soil hydraulic properties of the vadose zone, especially in more complex soil water models. This was demonstrated by (Wöhling & Vrugt, 2011), who used in situ measurements of SWC and pressure head at various depths in a heterogeneous vadose zone to calibrate 25 parameters of the Richards'-based HYDRUS-1D model with DREAM$_{(ZS)}$. While SWIM^2 already incorporates two different data sources for SWC in a SO approach, it could also benefit from a MO approach to make parameter estimates and soil moisture simulations even more accurate and precise. A possibility would be to add SWC and pressure head measurements at multiple depths to obtain better estimates of soil parameters as well as the RZ profile. However, this would incur more complex modeling and additional investment costs. Furthermore, high-resolution optical remote sensor data such as NDVI, LAI or FCOVER at 10 m resolution could be beneficial for estimating crop growth, and in turn resulting in better ET_a estimates (e.g., Pauwels et al., 2007). These data are freely accessible in real time and provided at a temporal resolution of several days, depending on cloud cover. While the relation between K_{cb} and vegetation indices have been studied for a long time (Choudhury et al., 1994), integrating optical remote sensing with modeling has only recently gained importance and has been demonstrated to be effective in estimating ET_a across diverse agricultural settings and crop types (Oliveira et al., 2024). Numerous studies showed potential improvement of the FAO-56 modeling approach by using crop information such as NDVI to have a better estimate crop growth parameters, including crop factors (K_{cb}) and crop growth stage lengths (L), and ET_a at field scale (Er-Raki et al., 2007; French et al., 2020; Hunsaker et al., 2005), while others did not observe significant improvements (El-Naggar et al., 2020). Additionally, a high-resolution surface soil moisture product from SAR remote sensing (e.g., Hajj et al. (2017)) could be assimilated to obtain a better estimate of the evaporative soil layer, while ET_a could potentially be calibrated using thermal infrared remote sensing imagery. Including these remote sensing data in the SWIM^2 framework using a MO approach could possibly improve parameter estimates.

6.3. Impact of Measurement Error Autocovariance

Although zero measurement error covariance is commonly assumed, this assumption is often incorrect and can significantly impact results, especially when measurements are biased. In previous studies, large error autocorrelations between 0.5 and 1 were found for soil moisture sensors at fixed positions, calculated based on soil moisture sensor measurements and spatial variability of the water retention curve (M. G. A. Hendrickx et al., 2023), and based on a pooled measurement error model approach (M. G. A. Hendrickx et al., 2025).

When biased and unbiased data sources were combined and all errors and error autocovariances are properly accounted for (reference scenario), the model was unbiased and precise. When measurement error covariance was

19447973, 2026, 2, Downloaded from https://agupubs.onlinelibrary.wiley.com/doi/10.1029/2025WR041324 by Forschungszentrum Jülich GmbH Research Center, Wiley Online Library on [17/05/2026]. See the Terms and Conditions (https://onlinelibrary.wiley.com/terms-and-conditions) on Wiley Online Library for rules of use; OA articles are governed by the applicable Creative Commons License

neglected (scenario B and E), model parameter uncertainty and soil moisture uncertainty estimates were substantially lower compared to when it was considered in the measurement error covariance matrix (scenario A and reference scenario). This underestimation of uncertainty results in a false sense of security and precision, as illustrated by the small model simulation uncertainty of scenario B compared to scenario A in Figure 11a, while considering the RMSD of the two scenarios in Figure 11b. In contrast, when measurement error covariance is considered but no unbiased measurements are integrated to correct for the biased measurement, the uncertainty estimates are large and represent the true uncertainty (scenario A). These findings highlight the importance of properly accounting for sensor errors and measurement error covariance in soil moisture modeling to avoid underestimation of parameter uncertainties and ensure more reliable predictions.

When measurement error (co)variance is unknown, DREAM$_{(ZS)}$ allows to calibrate error variance along with the uncertain model parameters. However, for uniform priors and an unknown measurement error autocorrelation structure, the Bayesian framework is not able to account for measurement bias, resulting in unrealistic small error variance estimates and biased soil moisture predictions. This error variance estimation was extended so that both the sensor error variance and autocorrelation are estimated (scenario F). Now, the unbiased soil samples allow for an accurate estimation of the entire sensor error covariance matrix, assuming a constant error variance and autocorrelation, leading to accurate soil moisture simulations and predictions, similar to the reference scenario.

6.4. Outlook

A promising application of the developed framework, SWIM^2, is its potential integration into manual and automated irrigation scheduling. Based on soil moisture predictions, farmers and water managers can make informed decisions to optimize water use and enhance crop productivity. A next step in the validation of SWIM^2 is the incorporation of uncertain weather forecasts into the framework. In a forecasting context, probabilistic weather forecasts, that is, ensemble predictions from numerical weather prediction models, can be used instead of historical weather data. The posterior parameter distribution obtained from MCMC can then be propagated through these ensembles, yielding predictive soil moisture distributions that account for both parameter and forcing uncertainty. Propagating both through the model allows us to assess how uncertainties interact and propagate through the soil water balance, thereby affecting both the predictive power and the associated prediction uncertainty of soil moisture estimates. Understanding these interactions is crucial for understanding and improving the reliability and usability of the framework in real-time decision-making. Future work could also include benchmarking the framework against more elaborated, distributed models based on Richards' equation to assess how increased spatial detail affects predictive performance and uncertainty propagation.

In addition, we argue that it is also worth investigating whether the framework can be applied effectively at regional or global scales for soil moisture, drought and irrigation requirement estimation and forecasting. At these larger scales, the use of coarser spatial and temporal resolutions introduces additional sources of uncertainty, such as representativeness errors associated with in situ measurements which arise because localized measurements may not adequately capture the variability within larger grid cells. A possible upscaling approach would be to distribute multiple sensor sets with IoT units across well-chosen locations within a grid cell, similar to how three sensors are currently used to estimate soil moisture at the field measurement zone or field scale. However, obtaining independent, unbiased soil samples for calibration at these larger scales presents a greater challenge. Nasta et al. (2025) discuss how a network of moderately instrumented monitoring sites with broad spatial coverage would enable us to capture state and variations in environmental conditions at these regional scales. To address these challenges, integrating supplementary data sources, such as SAR remote sensing of soil moisture, could be a promising direction, as it has already demonstrated its value at regional and global scales by providing continuous and spatially extensive soil moisture data (de Roos et al., 2024). High-resolution soil moisture products (e.g., Hajj et al. (2017)) could enable upscaling while maintaining a fine spatial resolution at the field scale. Incorporating these data into the inverse modeling framework could enhance its robustness and applicability by leveraging their spatial coverage while mitigating the limitations of in situ measurements.

19447973, 2026, 2, Downloaded from https://agupubs.onlinelibrary.wiley.com/doi/10.1029/2025WR041324 by Forschungszentrum Jülich GmbH Research Center, Wiley Online Library on [17/05/2026]. See the Terms and Conditions (https://onlinelibrary.wiley.com/terms-and-conditions) on Wiley Online Library for rules of use; OA articles are governed by the applicable Creative Commons License

7. Summary

This study demonstrates the effectiveness of the SWIM^2 framework for real-time soil moisture prediction during vegetable cropping cycles in Flanders, in which a low-dimensional soil water balance model with only 12 uncertain model parameters is calibrated efficiently and accurately with in situ soil moisture measurements, including (unbiased) soil moisture samples and (biased) continuous sensor data in a Bayesian inverse modeling framework using DREAM$_{(ZS)}$. The framework achieves soil moisture predictions for a 7-day prospect with an accuracy, that is, comparable to sensor accuracy (0.04 m^3 m^{-3}). A key strength of SWIM^2 is its adaptability, requiring only three sensors within a measurement zone of 80 m^2 and periodic unbiased soil samples to correct for sensor bias, while no prior information on soil parameters is needed. This positions SWIM^2 as a promising tool for optimizing water management and supporting agricultural decision-making across diverse conditions.

Both the continuous sensor data and periodic unbiased soil moisture samples play a key role in the high performance of SWIM^2. Leaving out one or the other results in lower accuracy and precision of soil moisture dynamics, or biased SWC estimates, respectively. Additionally, accounting for systematic sensor errors through the error covariance matrix is crucial for obtaining realistic uncertainty estimates and properly allocating weight to the different measurement types. Incorporating multi-objective approaches and external data sources such as remote sensing could further enhance the accuracy of soil moisture and evapotranspiration (ET_a) predictions. Potential applications of SWIM^2 range from automated field-scale irrigation scheduling to water management at broader regional scales.

Appendix A: Additional Figures

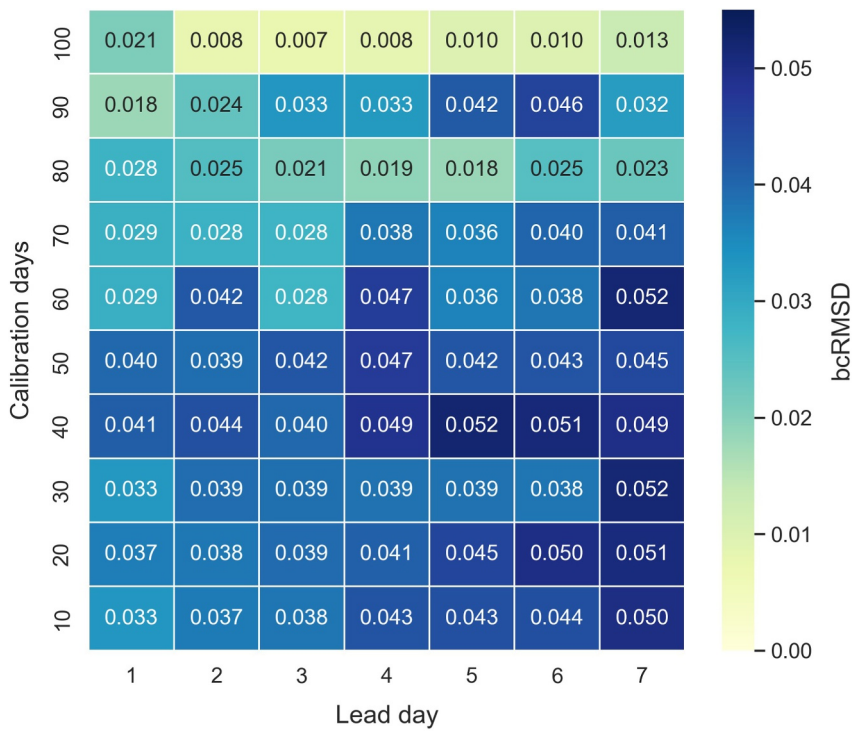

Figure A1. Heatmap of the bcRMSD during the validation period in function of the number of calibration days and lead day.

19447973, 2026, 2, Downloaded from https://agupubs.onlinelibrary.wiley.com/doi/10.1029/2025WR041324 by Forschungszentrum Jülich GmbH Research Center, Wiley Online Library on [17/05/2026]. See the Terms and Conditions (https://onlinelibrary.wiley.com/terms-and-conditions) on Wiley Online Library for rules of use; OA articles are governed by the applicable Creative Commons License

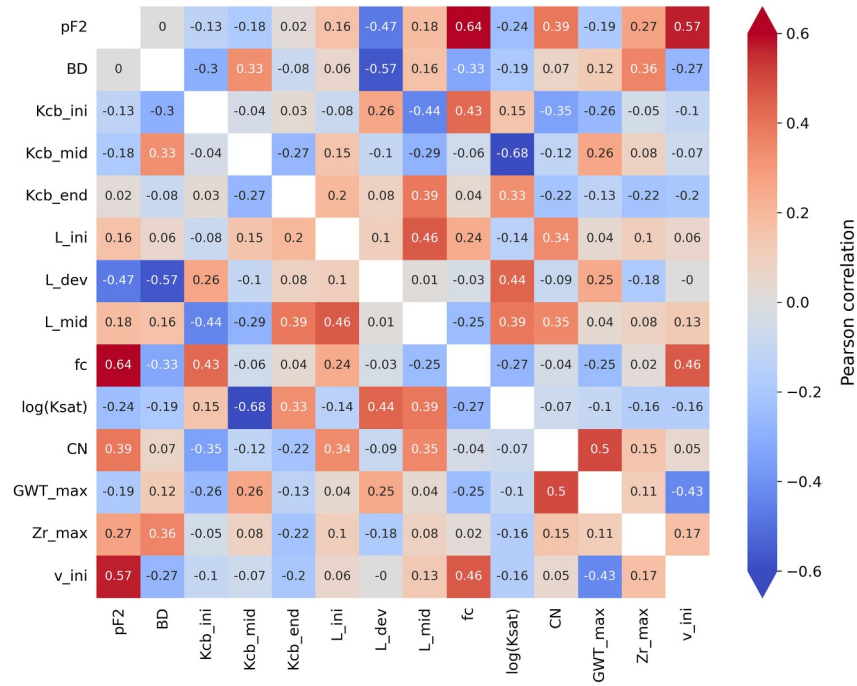

Figure A2. Correlation matrix heatmap of Pearson correlations between the posterior parameter distributions across all cases.

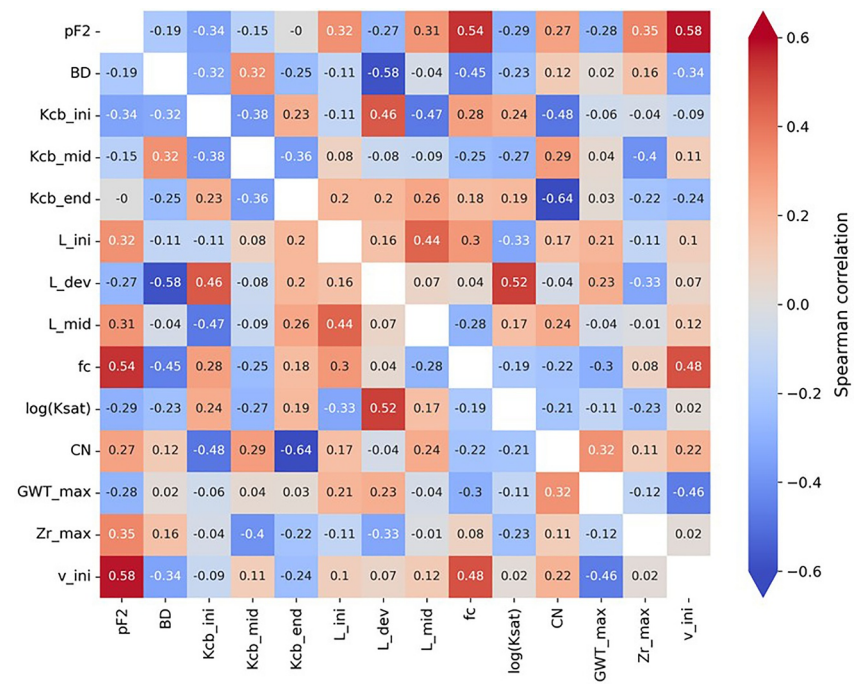

Figure A3. Correlation matrix heatmap of Spearman correlations between the posterior parameter distributions across all cases.

19447973, 2026, 2, Downloaded from https://agupubs.onlinelibrary.wiley.com/doi/10.1029/2025WR041324 by Forschungszentrum Jülich GmbH Research Center, Wiley Online Library on [17/05/2026]. See the Terms and Conditions (https://onlinelibrary.wiley.com/terms-and-conditions) on Wiley Online Library for rules of use; OA articles are governed by the applicable Creative Commons License

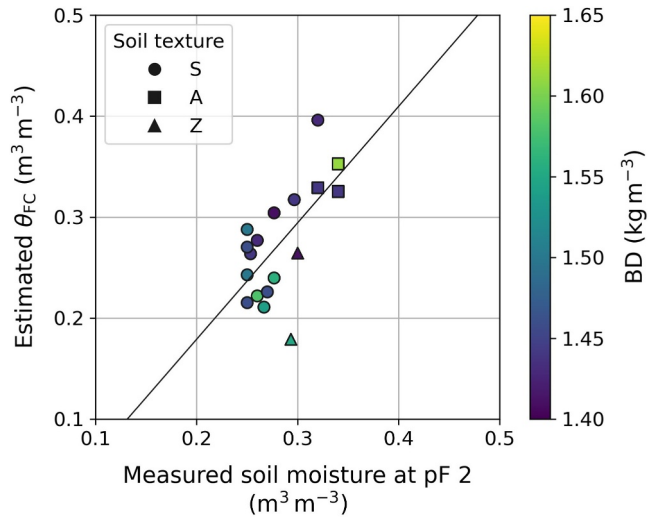

Figure A4. The final ML parameter estimate of SWC at field capacity (θ_{FC}) in function of the measured SWC at pF 2 based on soil cores, showing a good linear correlation of 0.64 ($y = 1.153\,x - 0.0515$). The soil map-based soil texture is indicated by the marker, and measured bulk density (BD, kg m^{-3}) is indicated by color.

Appendix B: DREAM$_{(ZS)}$ Configuration

The configuration of the DREAM$_{(ZS)}$ hyperparameters that was used in this study is shown in Table B1. The large amount of model simulations requires substantial CPU power. To obtain higher efficiency, the chains are run in parallel instead of serial. A multi-core implementation makes it possible to evaluate the N proposals simultaneously. In this case, six chains could be run in parallel on six logical processors.

Table B1
Configuration of DREAM$_{(ZS)}$

Hyperparameter	Value	Meaning
Par	12	Number of parameters (d)
seq	6	Number of chains (N)
T	4,000[a]	Number of generations per chain (T), with the total number of iterations equal to $N \times T$
	6,000[b]	
Thin	1	Thinning (<1 only required if high-dimensional)
steps	100	Steps in iteration
DEpairs	3	Number of chain pairs used to generate the jump (δ)
jr_scale[c]	0.8	Scaling of jumps (β)
Prior	"LHS"	Prior distribution: Uniform with Latin Hypercube Sampling for initialization
parallelUpdate	0.9	Mix of parallel direction (90%) and snooker jumps (10%)
Burn-in period	50%	Posterior distribution does not consider the first generations

[a]Cases with fast convergence. [b]Cases with slow convergence. [c]The user can enhance the acceptance rate by scaling the jump rate γ with a factor $\beta < 1$. This scaling will reduce the jumping distance, enhancing the acceptance rate and mixing of individual chains.

Appendix C: Numerical Experiment: Relation Between Error Variance, ACOR and LL

Numerical experiments were performed to assess the relation between the loglikelihood (LL), error autocorrelation (ACOR) and error variance (Var). A vector $\mathbf{E}$ containing $n = 10$ error residuals was randomly generated from a uniform distribution with values between −0.5 and 0.5, meaning that all errors are random and unbiased. The error variance and ACOR were ranging from 0.05 to 0.95 in steps of 0.05. For each Var-ACOR combination,

19447973, 2026, 2, Downloaded from https://agupubs.onlinelibrary.wiley.com/doi/10.1029/2025WR041324 by Forschungszentrum Jülich GmbH Research Center, Wiley Online Library on [17/05/2026]. See the Terms and Conditions (https://onlinelibrary.wiley.com/terms-and-conditions) on Wiley Online Library for rules of use; OA articles are governed by the applicable Creative Commons License

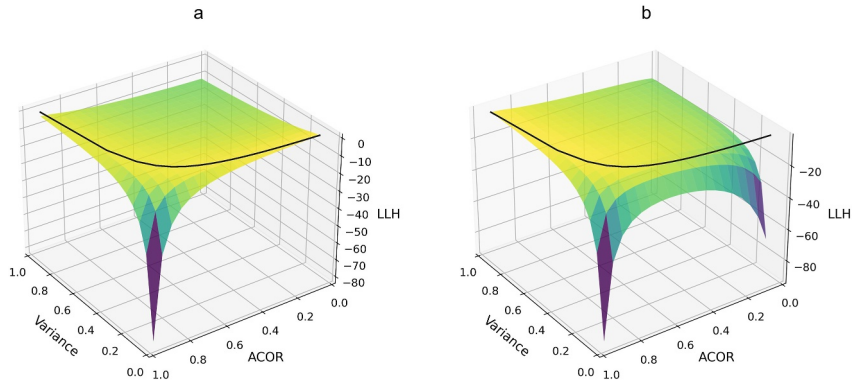

Figure C1. Surface plot of LL in function of error ACOR and error variance for a numerical experiment without (a) and with (b) bias between model and observations. The black line is an inverse hyperbolic relation between ACOR and Var, representing the theoretical maximum likelihood curve when no bias is present.

the error covariance matrix ($\mathbf{\Sigma}$) was constructed as a 10 by 10 matrix with the variance (Var) on the diagonal and the covariance (Cov = Var × ACOR) off-diagonal. The LL was then calculated for each error covariance matrix using a simplified formulation of Equation 6:

$$\mathrm{LL} = -\frac{n}{2}\ln(2\pi) - \frac{1}{2}\ln(|\mathbf{\Sigma}|) - \frac{1}{2}\mathbf{E}^{\mathrm{T}}\mathbf{\Sigma}^{-1}\mathbf{E},$$

where $\mathbf{E}$ represents the vector of error residuals, n is the number of error residuals, and $\mathbf{\Sigma}$ is the $n \times n$ error covariance matrix.

Since ACOR $= \frac{\mathrm{Cov}}{\mathrm{Var}}$, the relation between ACOR and Var is expected to be hyperbolic for a fixed Cov, with a high ACOR corresponding with a low Var and vice versa. However, the surface plot in Figure C1a shows that the likelihood decreases substantially for a low error Var in combination with a high error ACOR, while a high error ACOR is most likely in combination with a high error Var. In contrast, a low error ACOR is most likely when combined with a low error Var. In Bayesian inverse modeling algorithms such as DREAM$_{(ZS)}$, the LL function is the key objective function. As such, a higher LL results in a higher acceptance probability of the proposed parameter set. In Figure C1a, the maximum LL is observed as the inverse hyperbolic relation between ACOR and Var. If the error residuals $\mathbf{E}$ were randomly generated from a uniform distribution with values between 0.5 and 1.5, that is, mimicking a systematic error or bias of 1 between the model and the observations, a low ACOR in combination with low variance has a low likelihood (Figure C1b). This also corresponds to the Var-ACOR relation that was found in the posterior distribution in Scenario F (Figure 14).

Abbreviations

SWC	soil water content
RZ	root zone
SWB	soil water balance
DSS	decision support system
SWIM^2	Sensor Wielded Inverse Modeling of a Soil Water Irrigation Model
MZ	measurement zone
IoT	Internet-of-Things
DREAM$_{(ZS)}$	DiffeRential Evolution Adaptive Metropolis

19447973, 2026, 2, Downloaded from https://agupubs.onlinelibrary.wiley.com/doi/10.1029/2025WR041324 by Forschungszentrum Jülich GmbH Research Center, Wiley Online Library on [17/05/2026]. See the Terms and Conditions (https://onlinelibrary.wiley.com/terms-and-conditions) on Wiley Online Library for rules of use; OA articles are governed by the applicable Creative Commons License

Conflict of Interest

The authors declare no conflicts of interest relevant to this study.

Data Availability Statement

The soil moisture data and corresponding field data, including soil, irrigation and weather data, used for sensor-based modeling in this study are available at the KU Leuven RDR repository via https://doi.org/10.48804/FQAAAM, under a Creative Commons Attribution 4.0 International (CC BY 4.0) license. The data set includes continuous soil moisture sensor measurements (TEROS 10), gravimetric soil moisture samples, irrigation event records, soil physical properties, and weather data for 18 vegetable cropping cycles in Flanders, Belgium (2021–2023) (M. Hendrickx, Vanderborght, et al., 2025). The Python implementation of the SWIM² framework is openly available on GitHub under the GNU General Public License v3.0 (GPL-3.0), with an example case study provided, at: https://github.com/MaritHendrickx/SWIM2.

Acknowledgments

This work was funded by the Research Foundation Flanders (FWO fellowship 1S20822N). The study sites were monitored in the context of a project funded by Flanders innovation & entrepreneurship (VLAIO project HBC.2018.2201). We want to thank the farmers involved in this study. We acknowledge the support of the Soil Service of Belgium, who collected the field data, as well as their current and former researchers involved, Eveline Baens, Jonas Verellen, and Jarl Vaerten. We are also thanking the support of all research centers in Flanders as partners (*Provinciaal Proefcentrum voor de Groenteteelt Oost-Vlaanderen* (PCG), now Viaverda, *Proefstation voor de Groenteteelt* (PSKW), *Praktijkpunt Landbouw Vlaams-Brabant*), especially Elise Vandewoestijne, Joris De Nies, and Noémie Hisette. Thanks to the collaboration with Io-Things, we were able to assemble an optimal soil moisture sensor module to log and access real-time measurement data. In the preparation of the manuscript, AI tools were used for enhancing the readability and quality of the text. Open Access funding enabled and organized by Projekt DEAL.

References

Allen, R. G., Pereira, L. S., Raes, D., & Smith, M. (1998). Crop evapotranspiration. Guidelines for computing crop water requirements. In *Irrigation and drainage paper no. 56, FAO*. Food & Agriculture Organization of the United Nations (FAO).

Asadzadeh, M., & Tolson, B. (2013). Pareto archived dynamically dimensioned search with hypervolume-based selection for multi-objective optimization. *Engineering Optimization*, *45*(12), 1489–1509. https://doi.org/10.1080/0305215X.2012.748046

Bannister, R. N. (2008). A review of forecast error covariance statistics in atmospheric variational data assimilation. II: Modelling the forecast error covariance statistics. *Quarterly Journal of the Royal Meteorological Society*, *134*(637), 1971–1996. https://doi.org/10.1002/QJ.340

Bircher, S., Andreasen, M., Vuollet, J., Vehviläinen, J., Rautiainen, K., Jonard, F., et al. (2016). Soil moisture sensor calibration for organic soil surface layers. *Geoscientific Instrumentation, Methods and Data Systems*, *5*(1), 109–125. https://doi.org/10.5194/GI-5-109-2016

Bogena, H. R., Huisman, J. A., Schilling, B., Weuthen, A., Vereecken, H., Reemt Bogena, H., et al. (2017). Effective calibration of low-cost soil water content sensors. *Sensors*, *17*(1), 208. https://doi.org/10.3390/s17010208

Brinkhoff, J., Hornbuckle, J., & Ballester Lurbe, C. (2019). Soil moisture forecasting for irrigation recommendation. *IFAC-PapersOnLine*, *52*(30), 385–390. https://doi.org/10.1016/J.IFACOL.2019.12.586

Butts, M., & Graham, D. (2005). Flexible integrated watershed modeling with MIKE SHE. *Watershed Models*, 245–271. https://doi.org/10.1201/9781420037432.CH10

Cahn, M. D., Johnson, L. F., Alvino, A., Freire, M. I., & Ferreira, R. (2017). New approaches to irrigation scheduling of vegetables. *Horticulturae*, *3*(2), 28. https://doi.org/10.3390/horticulturae3020028

Choudhury, B. J., Ahmed, N. U., Idso, S. B., Reginato, R. J., & Daughtry, C. S. T. (1994). Relations between evaporation coefficients and vegetation indices studied by model simulations. *Remote Sensing of Environment*, *50*(1), 1–17. https://doi.org/10.1016/0034-4257(94)90090-6

Crow, W. T., & Van Loon, E. (2006). Impact of incorrect model error assumptions on the sequential assimilation of remotely sensed surface soil moisture. *Journal of Hydrometeorology*, *7*(3), 421–432. https://doi.org/10.1175/JHM499.1

De Lannoy, G. J. M., Bechtold, M., Busschaert, L., Heyvaert, Z., Modanesi, S., Dunmire, D., et al. (2024). Contributions of irrigation modeling, soil moisture and snow data assimilation to high-resolution water budget estimates over the Po basin: Progress towards digital replicas. *Journal of Advances in Modeling Earth Systems*, *16*(10), e2024MS004433. https://doi.org/10.1029/2024MS004433

de Roos, S., Bechtold, M., Busschaert, L., Lievens, H., & De Lannoy, G. J. M. (2024). Assimilation of Sentinel-1 backscatter to update AquaCrop estimates of soil moisture and crop biomass. *Journal of Geophysical Research: Biogeosciences*, *129*(10), e2024JG008231. https://doi.org/10.1029/2024JG008231

de Roos, S., Busschaert, L., Lievens, H., Bechtold, M., & De Lannoy, G. J. M. (2023). Optimisation of AquaCrop backscatter simulations using Sentinel-1 observations. *Remote Sensing of Environment*, *294*, 113621. https://doi.org/10.1016/J.RSE.2023.113621

Dong, Y., Miller, S., & Kelley, L. (2020). Performance evaluation of soil moisture sensors in Coarse- and fine-textured Michigan agricultural soils. *Agriculture*, *10*(12), 598. https://doi.org/10.3390/AGRICULTURE10120598

Dumont, B., Leemans, V., Mansouri, M., Bodson, B., Destain, J. P., & Destain, M. F. (2014). Parameter identification of the STICS crop model, using an accelerated formal MCMC approach. *Environmental Modelling & Software*, *52*, 121–135. https://doi.org/10.1016/J.ENVSOFT.2013.10.022

El-Naggar, A. G., Hedley, C. B., Horne, D., Roudier, P., & Clothier, B. E. (2020). Soil sensing technology improves application of irrigation water. *Agricultural Water Management*, *228*, 105901. https://doi.org/10.1016/j.agwat.2019.105901

Engeland, K., & Gottschalk, L. (2002). Bayesian estimation of parameters in a regional hydrological model. *Hydrology and Earth System Sciences*, *6*(5), 883–898. https://doi.org/10.5194/hess-6-883-2002

Er-Raki, S., Chehbouni, A., Guemouria, N., Duchemin, B., Ezzahar, J., & Hadria, R. (2007). Combining FAO-56 model and ground-based remote sensing to estimate water consumptions of wheat crops in a semi-arid region. *Agricultural Water Management*, *87*(1), 41–54. https://doi.org/10.1016/J.AGWAT.2006.02.004

Evin, G., Kavetski, D., Thyer, M., & Kuczera, G. (2013). Pitfalls and improvements in the joint inference of heteroscedasticity and autocorrelation in hydrological model calibration. *Water Resources Research*, *49*(7), 4518–4524. https://doi.org/10.1002/WRCR.20284

French, A. N., Hunsaker, D. J., Sanchez, C. A., Saber, M., Gonzalez, J. R., & Anderson, R. (2020). Satellite-based NDVI crop coefficients and evapotranspiration with eddy covariance validation for multiple durum wheat fields in the US southwest. *Agricultural Water Management*, *239*, 106266. https://doi.org/10.1016/J.AGWAT.2020.106266

Gallardo, M., Elia, A., & Thompson, R. B. (2020). Decision support systems and models for aiding irrigation and nutrient management of vegetable crops. In *Agricultural water management* (Vol. 240, p. 106209). Elsevier B.V. https://doi.org/10.1016/j.agwat.2020.106209

Gelman, A., & Rubin, D. B. (1992). Inference from iterative simulation using multiple sequences. *Statistical Science*, *7*(4), 457–472. https://doi.org/10.1214/ss/1177011136

George, K., & Soulis, K. X. (2012). Performance analysis and calibration of a new low-cost capacitance soil moisture sensor. *Journal of Irrigation and Drainage Engineering*, *138*(7), 632–641. https://doi.org/10.1061/(ASCE)IR.1943-4774.0000449

19447973, 2026, 2, Downloaded from https://agupubs.onlinelibrary.wiley.com/doi/10.1029/2025WR041324 by Forschungszentrum Jülich GmbH Research Center, Wiley Online Library on [17/05/2026]. See the Terms and Conditions (https://onlinelibrary.wiley.com/terms-and-conditions) on Wiley Online Library for rules of use; OA articles are governed by the applicable Creative Commons License

Goux, O., Weaver, A. T., Gürol, S., Guillet, O., & Piacentini, A. (2025). On the impact of observation error correlations in data assimilation, with application to along-track altimeter data. https://doi.org/10.1002/qj.5026

Grzenda, W. (2016). Informative versus non-informative prior distributions and their impact on the accuracy of Bayesian inference. *Statistics in Transition. New Series*, *17*(4), 763–780. https://doi.org/10.21307/stattrans-2016-051

Hajj, M. E., Baghdadi, N., Zribi, M., & Bazzi, H. (2017). Synergic use of Sentinel-1 and Sentinel-2 images for operational soil moisture mapping at high spatial resolution over agricultural areas. *Remote Sensing*, *9*(12), 1292. https://doi.org/10.3390/RS9121292

Hendrickx, M., Diels, J., Vanderborght, J., Bombeke, S., Matthyssen, E., Waverijn, A., & Janssens, P. (2025). Soil moisture measurements and field data from agricultural fields in Flanders (2021–2023). *KU Leuven RDR*. https://doi.org/10.48804/FQAAAM

Hendrickx, M. G. A., Diels, J., Janssens, P., Schlüter, S., & Vanderborght, J. (2023). Temporal covariance of spatial soil moisture variations: A mechanistic error modeling approach. *Vadose Zone Journal*, *23*(3), e20295. https://doi.org/10.1002/VZJ2.20295

Hendrickx, M. G. A., Vanderborght, J., Janssens, P., Bombeke, S., Matthyssen, E., Waverijn, A., & Diels, J. (2025). Pooled error variance and covariance estimation of sparse in situ soil moisture sensor measurements in agricultural fields in Flanders. *SOIL*, *11*(1), 435–456. https://doi.org/10.5194/SOIL-11-435-2025

Hu, G., & Dance, S. L. (2024). Sampling and misspecification errors in the estimation of observation-error covariance matrices using observation-minus-background and observation-minus-analysis statistics. *Quarterly Journal of the Royal Meteorological Society*, *150*(762), 3052–3077. https://doi.org/10.1002/QJ.4750

Hunsaker, D. J., Pinter, P. J., & Kimball, B. A. (2005). Wheat basal crop coefficients determined by normalized difference vegetation index. *Irrigation Science*, *24*(1), 1–14. https://doi.org/10.1007/S00271-005-0001-0

Jacques, D., Šimůnek, J., Timmerman, A., & Feyen, J. (2002). Calibration of Richards' and convection–dispersion equations to field-scale water flow and solute transport under rainfall conditions. *Journal of Hydrology*, *259*(1–4), 15–31. https://doi.org/10.1016/S0022-1694(01)00591-1

Janssens, P., Elsen, F., Elsen, A., Deckers, T., & Vandendriessche, H. (2011). Adapted soil water balance model for irrigation scheduling in "conference" pear orchards. *Acta Horticulturae*, *919*(5), 39–46. https://doi.org/10.17660/actahortic.2011.919

Kaptein, N. D., Light, M. E., & Savage, M. J. (2019). Review: Sensors for the improvement of irrigation efficiency in nurseries. *WaterSA*, *45*(3), 527–535. https://doi.org/10.4314/wsa.v45i3

Kavianihamedani, H., Quinn, J. D., & Smith, J. D. (2024). New diagnostic assessment of MCMC algorithm effectiveness, efficiency, reliability, and controllability. *IEEE Access*, *12*, 42385–42400. https://doi.org/10.1109/ACCESS.2024.3378752

Laloy, E., Fasbender, D., & Bielders, C. L. (2010). Parameter optimization and uncertainty analysis for plot-scale continuous modeling of runoff using a formal Bayesian approach. *Journal of Hydrology*, *380*(1–2), 82–93. https://doi.org/10.1016/J.JHYDROL.2009.10.025

Laloy, E., & Vrugt, J. A. (2012). High-dimensional posterior exploration of hydrologic models using multiple-try DREAM (ZS) and high-performance computing. *Water Resources Research*, *48*(1). https://doi.org/10.1029/2011WR010608

Langevin, C. D., Hughes, J. D., Banta, E. R., Niswonger, R. G., Panday, S., & Provost, A. M. (2017). Documentation for the MODFLOW 6 Groundwater Flow Model. *Techniques and Methods*. https://doi.org/10.3133/TM6A55

Mane, S., Das, N., Singh, G., Cosh, M., & Dong, Y. (2024). Advancements in dielectric soil moisture sensor Calibration: A comprehensive review of methods and techniques. *Computers and Electronics in Agriculture*, *218*, 108686. https://doi.org/10.1016/J.COMPAG.2024.108686

METER Group. (2018). TEROS 10. *The Manual*. Retrieved from http://publications.metergroup.com/Manuals/20788_TEROS10_Manual_Web.pdf

Nasta, P., Blöschl, G., Bogena, H. R., Zacharias, S., Baatz, R., De Lannoy, G., et al. (2025). HESS opinions: Towards a common vision for the future of hydrological observatories. *Hydrology and Earth System Sciences*, *29*(2), 465–483. https://doi.org/10.5194/HESS-29-465-2025

Nasta, P., Coccia, F., Lazzaro, U., Bogena, H. R., Huisman, J. A., Sica, B., et al. (2024). Temperature-corrected calibration of GS3 and TEROS-12 soil water content sensors. *Sensors*, *24*(3), 952. https://doi.org/10.3390/S24030952

Nemali, K. S., Montesano, F., Dove, S. K., & van Iersel, M. W. (2007). Calibration and performance of moisture sensors in soilless substrates: ECH2O and Theta probes. *Scientia Horticulturae*, *112*(2), 227–234. https://doi.org/10.1016/j.scienta.2006.12.013

Obaideen, K., Yousef, B. A. A., AlMallahi, M. N., Tan, Y. C., Mahmoud, M., Jaber, H., & Ramadan, M. (2022). An overview of smart irrigation systems using IoT. *Energy Nexus*, *7*, 100124. https://doi.org/10.1016/J.NEXUS.2022.100124

O'Grady, M. J., & O'Hare, G. M. P. (2017). Modelling the smart farm. *Information Processing in Agriculture*, *4*(3), 179–187. https://doi.org/10.1016/J.INPA.2017.05.001

Oliveira, W. M. K., Maggi, M. F., Venancio, L. P., Bazzi, C. L., Nobrega, L. H. P., Oliveira, A. S. D. M., et al. (2024). Remote sensing-based algorithms for estimating evapotranspiration in agricultural systems: A systematic literature review. *IEEE Geoscience and Remote Sensing Magazine*, *12*(4), 190–217. https://doi.org/10.1109/MGRS.2024.3469182

Paige, G. B., & Keefer, T. O. (2008). Comparison of field performance of multiple soil moisture sensors in a semi-arid rangeland. *Journal of the American Water Resources Association*, *44*(1), 121–135. https://doi.org/10.1111/j.1752-1688.2007.00142.x

Pauwels, V. R. N., & De Lannoy, G. J. M. (2015). Error covariance calculation for forecast bias estimation in hydrologic data assimilation. *Advances in Water Resources*, *86*, 284–296. https://doi.org/10.1016/J.ADVWATRES.2015.05.013

Pauwels, V. R. N., De Lannoy, G. J. M., Hendricks Franssen, H.-J., & Vereecken, H. (2013). Simultaneous estimation of model state variables and observation and forecast biases using a two-stage hybrid Kalman filter. *Hydrology and Earth System Sciences*, *17*(9), 3499–3521. https://doi.org/10.5194/hess-17-3499-2013

Pauwels, V. R. N., Verhoest, N. E. C., De Lannoy, G. J. M., Guissard, V., Lucau, C., & Defourny, P. (2007). Optimization of a coupled hydrology–crop growth model through the assimilation of observed soil moisture and leaf area index values using an ensemble Kalman filter. *Water Resources Research*, *43*(4), 4421. https://doi.org/10.1029/2006WR004942

Pereira, L. S., Paredes, P., & Jovanovic, N. (2020). Soil water balance models for determining crop water and irrigation requirements and irrigation scheduling focusing on the FAO56 method and the dual K c approach. *Agricultural Water Management*, *241*, 106357. https://doi.org/10.1016/j.agwat.2020.106357

Raes, D. (2002). BUDGET: A soil water and salt balance model. *Reference Manual, Version 5*.

Raes, D., Steduto, P., Hsiao, T. C., & Fereres, E. (2009). Aquacrop-The FAO crop model to simulate yield response to water: II. Main algorithms and software description. *Agronomy Journal*, *101*(3), 438–447. https://doi.org/10.2134/agronj2008.0140s

Reichle, R. H., & Koster, R. D. (2004). Bias reduction in short records of satellite soil moisture. *Geophysical Research Letters*, *31*(19). https://doi.org/10.1029/2004GL020938

Richards, M. (2015). PyETo: Python package for calculating reference/potential evapotranspiration (ETo). Retrieved from https://github.com/woodcrafty/PyETo

Ritter, A., Hupet, F., Muñoz-Carpena, R., Lambot, S., & Vanclooster, M. (2003). Using inverse methods for estimating soil hydraulic properties from field data as an alternative to direct methods. *Agricultural Water Management*, *59*(2), 77–96. https://doi.org/10.1016/S0378-3774(02)00160-9

19447973, 2026, 2, Downloaded from https://agupubs.onlinelibrary.wiley.com/doi/10.1029/2025WR041324 by Forschungszentrum Jülich GmbH Research Center, Wiley Online Library on [17/05/2026]. See the Terms and Conditions (https://onlinelibrary.wiley.com/terms-and-conditions) on Wiley Online Library for rules of use; OA articles are governed by the applicable Creative Commons License

Scharnagl, B., Iden, S. C., Durner, W., Vereecken, H., & Herbst, M. (2015). Inverse modelling of in situ soil water dynamics: Accounting for heteroscedastic, autocorrelated, and non-Gaussian distributed residuals. *Hydrology and Earth System Sciences Discussions*, *12*, 2155–2199. https://doi.org/10.5194/hessd-12-2155-2015

Scharnagl, B., Vrugt, J. A., Vereecken, H., & Herbst, M. (2011). Inverse modelling of in situ soil water dynamics: Investigating the effect of different prior distributions of the soil hydraulic parameters. *Hydrology and Earth System Sciences*, *15*(10), 3043–3059. https://doi.org/10.5194/HESS-15-3043-2011

Schübl, M., Stumpp, C., & Brunetti, G. (2022). A Bayesian perspective on the information content of soil water measurements for the hydrological characterization of the vadose zone. *Journal of Hydrology*, *613*, 128429. https://doi.org/10.1016/J.JHYDROL.2022.128429

Simunek, J., Van Genuchten, M. T., & Sejna, M. (2005). The HYDRUS-1D software package for simulating the one-dimensional movement of water, heat, and multiple solutes in variably-saturated media. University of California-Riverside Research Reports, 3 (pp. 1–240).

Soil Conservation Service (SCS). (1964). Section 4: Hydrology. In *National engineering handbook*. Department of Agriculture.450.

Soulis, K. X., Elmaloglou, S., & Dercas, N. (2015). Investigating the effects of soil moisture sensors positioning and accuracy on soil moisture based drip irrigation scheduling systems. *Agricultural Water Management*, *148*, 258–268. https://doi.org/10.1016/J.AGWAT.2014.10.015

Steduto, P., Hsiao, T. C., Raes, D., & Fereres, E. (2009). AquaCrop—The FAO crop model to simulate yield response to water: I. Concepts and underlying principles. *Agronomy Journal*, *101*(3), 426–437. https://doi.org/10.2134/agronj2008.0139s

Stewart, L. M., Dance, S. L., & Nichols, N. K. (2008). Correlated observation errors in data assimilation. *International Journal for Numerical Methods in Fluids*, *56*(8), 1521–1527. https://doi.org/10.1002/FLD.1636

Ter Braak, C. J. F., & Vrugt, J. A. (2008). Differential evolution Markov Chain with snooker updater and fewer chains. *Statistics and Computing*, *18*(4), 435–446. https://doi.org/10.1007/s11222-008-9104-9

Thompson, R. B., Delcour, I., Berkmoes, E., & Stavridou, E. (Eds.). (2018). *The Fertigation Bible*.

Van Dam, J. C., Huygen, J., Wesseling, J. G., Feddes, R. A., Kabat, P., Van Walsum, P. E. V., et al. (1997). *Theory of SWAP version 2.0; Simulation of water flow, solute transport and plant growth in the soil-water-atmosphere-plant environment*. DLO Winand Staring Centre.

Van Dongen, S. (2006). Prior specification in Bayesian statistics: Three cautionary tales. *Journal of Theoretical Biology*, *242*(1), 90–100. https://doi.org/10.1016/J.JTBI.2006.02.002

Varble, J. L., & Chávez, J. L. (2011). Performance evaluation and calibration of soil water content and potential sensors for agricultural soils in eastern Colorado. *Agricultural Water Management*, *101*(1), 93–106. https://doi.org/10.1016/j.agwat.2011.09.007

Vaz, C. M. P., Jones, S., Meding, M., & Tuller, M. (2013). Evaluation of standard calibration functions for eight electromagnetic soil moisture sensors. *Vadose Zone Journal*, *12*(2), vzj2012-0160. https://doi.org/10.2136/VZJ2012.0160

Vereecken, H., Huisman, J. A., Bogena, H., Vanderborght, J., Vrugt, J. A., & Hopmans, J. W. (2008). On the value of soil moisture measurements in vadose zone hydrology: A review. *Water Resources Research*, *44*(4). https://doi.org/10.1029/2008WR006829

Vrugt, J. A. (2016). Markov chain Monte Carlo simulation using the DREAM software package: Theory, concepts, and MATLAB implementation. *Environmental Modelling & Software*, *75*, 273–316. https://doi.org/10.1016/j.envsoft.2015.08.013

Vrugt, J. A., Ter Braak, C. J. F., Clark, M. P., Hyman, J. M., Robinson, B. A., Ter Braak, C. J. F., et al. (2008). Treatment of input uncertainty in hydrologic modeling: Doing hydrology backward with Markov chain Monte Carlo simulation. *Water Resources Research*, *44*(12). https://doi.org/10.1029/2007wr006720

Vrugt, J. A., Ter Braak, C. J. F., Diks, C. G. H., Robinson, B. A., Hyman, J. M., & Higdon, D. (2009). Accelerating Markov chain Monte Carlo simulation by differential evolution with self-adaptive randomized subspace sampling. *International Journal of Nonlinear Sciences and Numerical Stimulation*, *10*(3), 273–290. https://doi.org/10.1515/IJNSNS.2009.10.3.273

Wang, W., Wei, Y., Hao, L., Wei, Z., & Zhao, T. (2025). Soil moisture forecasting in wireless sensor networks via spatiotemporal graph convolutional networks. *Vadose Zone Journal*, *24*(1), e70000. https://doi.org/10.1002/VZJ2.70000

Wang, X., Wang, X. S., Li, N., & Wan, L. (2021). Bayesian inversion of soil hydraulic properties from simplified evaporation experiments: Use of DREAM(ZS) algorithm. *Water*, *13*(19), 2614. https://doi.org/10.3390/W13192614

Wöhling, T., & Vrugt, J. A. (2011). Multiresponse multilayer vadose zone model calibration using Markov chain Monte Carlo simulation and field water retention data. *Water Resources Research*, *47*(4), 4510. https://doi.org/10.1029/2010WR009265

Wöhling, T., Vrugt, J. A., & Barkle, G. F. (2008). Comparison of three multiobjective optimization algorithms for inverse modeling of vadose zone hydraulic properties. *Soil Science Society of America Journal*, *72*(2), 305–319.

Zambon, I., Cecchini, M., Egidi, G., Saporito, M. G., & Colantoni, A. (2019). Revolution 4.0: Industry vs. Agriculture in a future development for SMEs. *Processes 2019*, *7*(1), 36. https://doi.org/10.3390/PR7010036

19447973, 2026, 2, Downloaded from https://agupubs.onlinelibrary.wiley.com/doi/10.1029/2025WR041324 by Forschungszentrum Jülich GmbH Research Center, Wiley Online Library on [17/05/2026]. See the Terms and Conditions (https://onlinelibrary.wiley.com/terms-and-conditions) on Wiley Online Library for rules of use; OA articles are governed by the applicable Creative Commons License